© 2019. Published by The Company of Biologists Ltd | Development (2019) 146, dev167882. doi:10.1242/dev.167882

RESEARCH ARTICLE

Bone morphology is regulated modularly by global and regional genetic programs

Shai Eyal[1], Shiri Kult[1], Sarah Rubin[1], Sharon Krief[1], Neta Felsenthal[1], Kyriel M. Pineault[2], Dena Leshkowitz[3], Tomer-Meir Salame[3], Yoseph Addadi[3], Deneen M. Wellik[2] and Elazar Zelzer[1,*]

ABSTRACT

Bone protrusions provide stable anchoring sites for ligaments and tendons and define the unique morphology of each long bone. Despite their importance, the mechanism by which superstructures are patterned is unknown. Here, we identify components of the genetic program that control the patterning of *Sox9*$^+$/*Scx*$^+$ superstructure progenitors in mouse and show that this program includes both global and regional regulatory modules. Using light-sheet fluorescence microscopy combined with genetic lineage labeling, we mapped the broad contribution of the *Sox9*$^+$/*Scx*$^+$ progenitors to the formation of bone superstructures. Then, by combining literature-based evidence, comparative transcriptomic analysis and genetic mouse models, we identified *Gli3* as a global regulator of superstructure patterning, whereas *Pbx1*, *Pbx2*, *Hoxa11* and *Hoxd11* act as proximal and distal regulators, respectively. Moreover, by demonstrating a dose-dependent pattern regulation in *Gli3* and *Pbx1* compound mutations, we show that the global and regional regulatory modules work in a coordinated manner. Collectively, our results provide strong evidence for genetic regulation of superstructure patterning, which further supports the notion that long bone development is a modular process.

This article has an associated 'The people behind the papers' interview.

KEY WORDS: Cartilage, Patterning, Morphology, Superstructure, Sox9, Scleraxis, Modularity, Gli3, Pbx, Hox, Mouse

INTRODUCTION

The vertebrate skeleton is composed of numerous bones, each displaying a unique shape and size. Yet, despite this morphological diversity, most bones are formed by a common developmental process, namely endochondral ossification (Berendsen and Olsen, 2015; Cervantes-Diaz et al., 2017; Long and Ornitz, 2013; Olsen et al., 2000). During this process, mesenchymal cells derived from the lateral plate mesoderm under the regulation of the transcription factor SRY-box 9 (SOX9) condense and differentiate into chondroprogenitors, forming the cartilaginous anlage of the future bones (Kawakami et al., 2006; Zhao et al., 1997). Next, a cascade of chondrocyte differentiation steps will give rise to growth plates on both proximal and distal ends of the anlage. Subsequently, blood vessels and bone-building cells, termed osteoblasts, invade the cartilage anlage and drive ossification of the cartilaginous template from the mid-shaft, pursuing the progression of the growth plates (Kronenberg, 2003).

Endochondral ossification has been studied extensively for more than two centuries, generating a vast amount of information on this process. Nevertheless, mechanisms that grant each bone with its distinctive shape are missing. A hallmark of the unique morphology of each long bone is the superstructures that protrude from its surface known as bone eminences, such as the greater and deltoid tuberosities, greater and lesser trochanters, etc., and condyles, such as the distal lateral and medial epicondyles of the humerus. One of the main functions of bone superstructures is to provide an attachment point for tendons and ligaments, which transmit force from the contracting muscles to the skeleton (Lessa et al., 2008; McHenry and Corruccini, 1975; Polly, 2007).

Interestingly, it was previously shown that the site where tendon attaches to bone is formed by a unique set of progenitors that co-express *Sox9* and scleraxis (*Scx*) (Blitz et al., 2013; Sugimoto et al., 2013). Moreover, it was demonstrated that cells that contribute to the bony side of the attachment do not descend from the cells that create the bone shaft anlage, but are specified after them. Finally, it was demonstrated that these unique progenitors are specifically regulated by the TGFβ and BMP signaling pathways (Blitz et al., 2009, 2013). In addition to providing a mechanism for the development of tendon-to-bone attachment site, these findings also offer an alternative, modular model for long bone development. According to this model, one set of *Sox9*$^+$ cells forms the cylindrical anlage of the future bone shaft, which will serve as the bone substructure, whereas a second pool of *Sox9*$^+$/*Scx*$^+$ cells will be added onto this substructure to give rise to the different superstructures.

Current literature provides ample evidence in support of the modular model of long bone development, which is based on lineage tracing, temporal initiation and cell differentiation of the *Sox9*$^+$/*Scx*$^+$ progenitor cells. However, this model is still missing the mechanisms that regulate the early patterning of the *Sox9*$^+$/*Scx*$^+$ progenitor cells, such that superstructures will form on the developing long bone at the right location, and with the correct shape and size. In this study, we examine the regulatory mechanisms underlying these aspects of modularity in skeletal development. Three-dimensional (3D) reconstruction of different long bones and their protruding superstructures allowed us to demonstrate modularity in long bone development. Comparative transcriptomic analysis and loss-of-function assays showed that GLI-Kruppel family member (*Gli3*) globally regulates the spatial organization of the *Sox9*$^+$/*Scx*$^+$ progenitors in both forelimb and hindlimb, whereas homeobox a11 (*Hoxa11*) and *Hoxd11* regulate patterning of distal superstructures and pre-B cell leukemia homeobox 1 (*Pbx1*) and *Pbx2* regulate proximal superstructure progenitors. Overall, we provide cellular evidence for the existence of a patterning mechanism that involves both global and regional regulation and highlight some of the genes that facilitate the patterning of superstructures along the developing long bones.

[1]Weizmann Institute of Science, Department of Molecular Genetics, Rehovot 76100, Israel. [2]University of Wisconsin-Madison, Department of Cell & Regenerative Biology, Madison, WI 53705, USA. [3]Weizmann Institute of Science, Department of Life Sciences Core Facilities, Rehovot 76100, Israel.

*Author for correspondence (eli.zelzer@weizmann.ac.il)

S.E., 0000-0001-8131-8077; D.M.W., 0000-0003-4078-8560; E.Z., 0000-0002-1584-6602

Received 16 May 2018; Accepted 13 June 2019

Development (2019) 146, dev167882. doi:10.1242/dev.167882

RESULTS

Sox9$^+$/*Scx*$^+$ superstructure progenitors contribute extensively to the morphology of long bone anlagen

To understand better the scope of modularity in long bone morphogenesis, we performed pulse-chase cell-lineage experiments by crossing either *Sox9-CreER*^{T2} or collagen type II alpha 1 (*Col2a1*)-*CreER*^{T2} transgenic reporter mice with *Rosa26-tdTomato* reporter mice (Madisen et al., 2010; Nakamura et al., 2006; Soeda et al., 2010). Pregnant females were administered a single dose of 0.03 mg/g tamoxifen/body weight at either embryonic day (E) 10.5 or E11.5. Previously, we showed that this time window allows the exclusive labeling of cells of the cylindrical bone substructure, leaving the superstructure cells unlabeled (described in detail by Blitz et al., 2013; Eyal et al., 2015). To map comprehensively the unlabeled superstructure cells in different skeletal elements, we have established a 3D imaging pipeline that includes clearing of the labeled limbs optically, light-sheet fluorescence microscopy and, finally, reconstruction of obtained images into a 3D object (Treweek et al., 2015; Yang et al., 2014). To visualize the superstructures better, whole-mount limbs were immunostained for COL2A1.

As seen in Fig. 1A,B (and Movies 1-3), in E14.5 *Sox9-tdTomato*$^+$ or E15.5 *Col2a1-tdTomato*$^+$ limbs, all superstructures of different long bones were *tdTomato* negative, including greater, lesser and deltoid tuberosities, olecranon, and greater, lesser and third trochanters. Interestingly, in addition to bone eminences, we observed various condyles and sesamoid bones that were also *tdTomato* negative, including distal medial and lateral humeral epicondyles, medial tibial condyle, patella, and medial and lateral fabella. These results demonstrate the generality of the modular process of long bone morphogenesis in the limb.

To demonstrate this modularity further, we examined sagittal and coronal sections of E13.5 fore- and hindlimbs from *ScxGFP* transgenic embryos (Pryce et al., 2007) that were stained using antibodies against SOX9. As seen in Fig. 1C, we observed an abundance of SOX9$^+$ and *Scx*$^+$ double-positive cells at anatomical locations of various future superstructures along the shafts of different bones. Taken together, these results indicate the extensive contribution of *Sox9*$^+$/*Scx*$^+$ superstructure progenitors to the 3D morphology of cartilaginous anlagen, highlighting the modularity of this process both temporally and from lineage analyses.

Gli3 is a global regulator of *Sox9*$^+$/*Scx*$^+$ progenitors patterning during superstructure development

An immediate implication of the modular model is the existence of a mechanism that regulates the patterning of the *Sox9*$^+$/*Scx*$^+$ progenitors to position the superstructure correctly along the bone substructure. To uncover this mechanism, we first searched the literature for mutations leading to observable superstructure patterning abnormalities. We found that the skeletons of *Gli3*-null embryos, previously known as extra toes (*Xt*), exhibit a variety of superstructure abnormalities (Johnson, 1967). To characterize these defects, we crossed *Gli3* heterozygous mice and examined skeletal preparations from E17.5 embryos. As seen in Fig. 2A-I, both fore- and hindlimbs of *Gli3*^{null} embryos exhibited numerous dysplastic superstructures, including lesser and deltoid tuberosity, olecranon, patella, and additional ectopic sesamoids. Notably, the aberrant

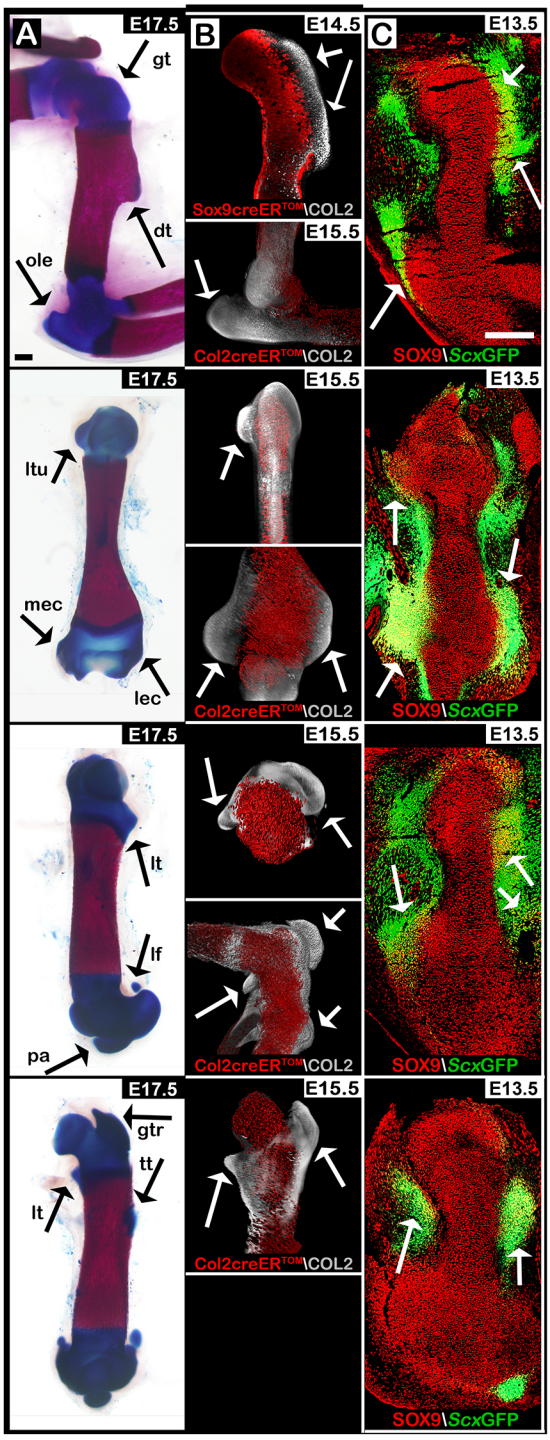

Fig. 1. Long bone morphology is affected extensively by numerous pools of *Sox9*$^+$/*Scx*$^+$ progenitors. Images showing sagittal and coronal views of the superstructures that form along the forelimb and hindlimb long bones. (A) Skeletal preparations of E17.5 wild-type limbs. Superstructures are indicated by black arrows. (B) Maximum intensity projection (MIP) images of E14.5 forelimb from *Sox9-Cre*^{ER}*-tdTomato* transgenic embryos and E15.5 fore- and hindlimbs from *Col2a1-Cre*^{ER}*-tdTomato* transgenic embryos. Whole-mount limbs were stained against COL2A1, imaged using light-sheet microscopy and reconstructed. Whereas first-wave *Sox9*$^+$ progenitors were labeled by *tdTomato*, the secondary wave of *Sox9*$^+$/*Scx*$^+$ progenitors remained unstained. *tdTomato*$^-$ precursors contributed exclusively to superstructure formation (white arrows). (C) Sagittal and coronal sections through E13.5 fore- and hindlimbs from *ScxGFP* transgenic embryos stained against SOX9. SOX9 and *Scx* co-expressing cells are indicated by white arrows. Sagittal sections in first and third rows; coronal sections in second and fourth rows. dt, deltoid tuberosity; gt, greater tuberosity; gtr, greater trochanter; lec, lateral epicondyle; lf, lateral fabella; lt, lesser trochanter; ltu, lesser tuberosity; mec, medial epicondyle; ole, olecranon; pa, patella; tt, third trochanter. Scale bars: 200 µm.

Development (2019) 146, dev167882. doi:10.1242/dev.167882

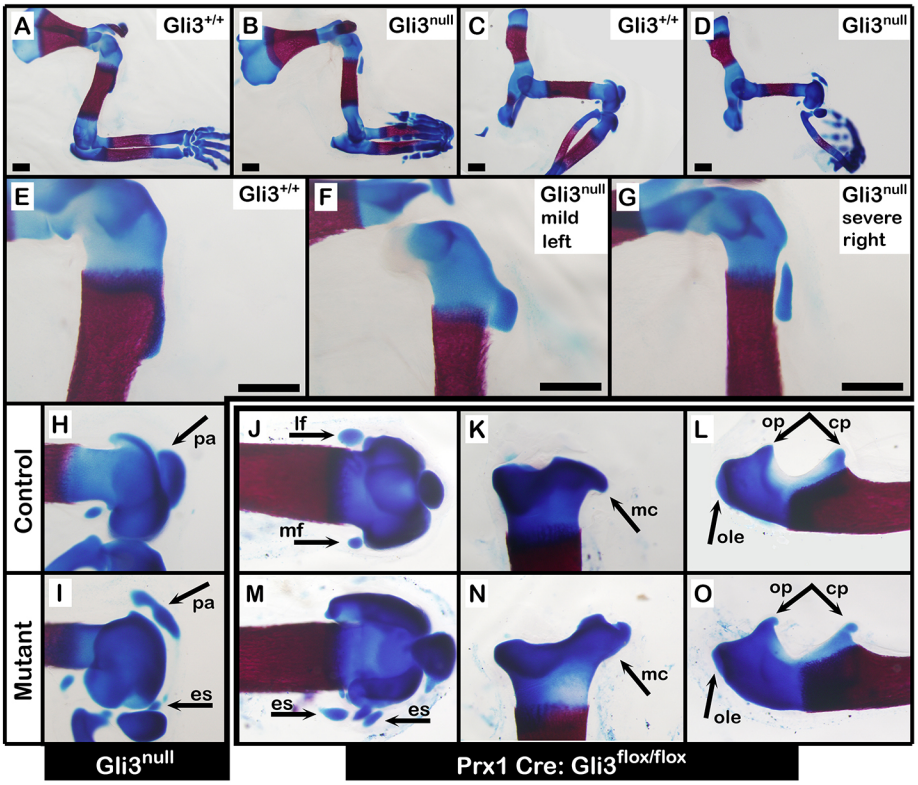

Fig. 2. *Gli3* regulates the patterning of superstructures globally. (A-O) Skeletal preparations of E17.5 fore- and hindlimbs from *Gli3* KO and control embryos (A-I) and from limb-specific *Prx1-Cre;Gli3*^{floxed} cKO and control embryos (J-O). Affected superstructures are indicated by black arrows. cp, coronoid process; es, ectopic sesamoids; lf, lateral fabella; mc, medial tibial condyle; mf, medial fabella; ole, olecranon; op, olecranon process; pa, patella. Scale bars: 500 µm.

patterning of the deltoid tuberosity ranged in severity from mildly abnormal morphology to complete separation from the humeral shaft (compare left and right forelimbs in Fig. 2F and 2G, respectively) (Table S1). We also examined *Prx1-Cre;Gli3*$^{fl/fl}$ embryos, in which *Gli3* was conditionally knocked out (cKO) in limb mesenchyme (Blaess et al., 2008; Logan et al., 2002). Similar to *Gli3*^{null} mutants, limb-specific *Gli3* cKO also resulted in diverse abnormally patterned superstructures, such as induction of supernumerary sesamoids around the knee, dysplastic medial tibial condyle and dysplastic ulnar olecranon and coronoid processes (Fig. 2J-O).

To study the possibility that *Gli3* regulates the patterning of superstructure progenitors, we sought to examine the distribution of *Sox9*$^{+}$/*Scx*$^{+}$ cells in *Gli3*^{null} limbs. For that, we crossed heterozygous *Gli3* mice with *Gli3*$^{+/-}$; *ScxGFP* transgenic reporter mice and stained sagittal sections of E13.5 fore- and hindlimbs against SOX9 to highlight chondrocytes. As seen in Fig. 3A-F, the spatial distribution of *Sox9*$^{+}$/*Scx*$^{+}$ progenitors in *Gli3*^{null} limbs was abnormal. Whereas in control limbs these progenitors were patterned in juxtaposition to the humeral shaft (Fig. 3A, dotted line), in the mutant these cells were laterally spread and less condensed (Fig. 3D, dotted line). To understand how the abnormal distribution of *Sox9*$^{+}$/*Scx*$^{+}$ progenitors translates into superstructure abnormality, we examined the spatiotemporal differentiation of deltoid tuberosity precursors in E13.5 and E16.5 sagittal sections from control and *Gli3* KO forelimbs. Sections were stained using antibodies against SOX9 and COL2A1, a marker for differentiated chondrocytes (Fig. 3G-L). As expected, at E13.5 we repeatedly observed the lateral spreading of deltoid tuberosity precursors (Fig. 3H,I, dotted lines). Moreover, we noticed that the degree of cellular lateralization varied both in pattern and in distance from the humeral shaft (Fig. 3H,I, white bars). At E16.5, the abnormal deltoid tuberosity morphologies were clearly evident and ranged from dysplastic to separate deltoid tuberosity (Fig. 3K and 3L, respectively). We concluded that *Gli3* is necessary for correct spatial organization of deltoid tuberosity *Sox9*$^{+}$/*Scx*$^{+}$ precursors and, thus, for superstructure patterning.

The finding that *Gli3* regulates superstructure patterning raises the question whether *Gli3* acts autonomously within the *Sox9*$^{+}$/*Scx*$^{+}$ progenitors. To directly examine whether *Gli3* operates autonomously within the *Sox9*$^{+}$/*Scx*$^{+}$ progenitor population, we blocked the expression of *Gli3* in *Scx*- or *Sox9*-expressing cells by crossing *Scx-Cre* or *Sox9-Cre* mice to *Gli3*$^{fl/fl}$ mice. As seen in Fig. 4, skeletal preparation of both *Scx-Cre;Gli3*$^{fl/fl}$ (Fig. 4A-B′) and *Sox9-Cre;Gli3*$^{fl/fl}$ cKOs (Fig. 4C-D′) revealed hypoplasia of the deltoid tuberosity and lateral fabella. In addition, we observed dysplasia of the patella in *Sox9-Cre;Gli3*$^{fl/fl}$ mutants (Fig. 4D′). This finding clearly indicates an autonomous role of *Gli3* in superstructure patterning; yet, the milder phenotypes that we observed in the skeletons of both *Scx-Cre;Gli3*$^{fl/fl}$ and *Sox9-Cre;Gli3*$^{fl/fl}$ cKOs relative to the *Gli3*^{null} mice suggest a potential additional, non-autonomous effect of *Gli3* in superstructure patterning.

Comparative transcriptomic analysis of proximal and distal *Sox9*$^{+}$/*Scx*$^{+}$ progenitors predicts regional regulation of superstructure patterning

Although *Gli3* had a global effect on superstructure patterning, we suspected that regional regulatory circuitry also exists, such that patterning of specific superstructures could be regulated independently. To search for genes potentially involved in this mechanism, we developed a protocol for prospective isolation of *Sox9-tdTomato*$^{+}$/*ScxGFP*$^{+}$ progenitors by fluorescence-activated cell sorting (FACS). Moreover, to enable distinction between global and regional patterning regulators, we designed our system to allow separate isolation of proximal and distal cell populations. To this end, we crossed *Sox9-CreER*^{T2}*;Rosa26-tdTomato* reporter mice with *ScxGFP* transgenic reporter mice. Pregnant females were administered a single dose of 0.03 mg/g tamoxifen/body weight at

Development (2019) 146, dev167882. doi:10.1242/dev.167882

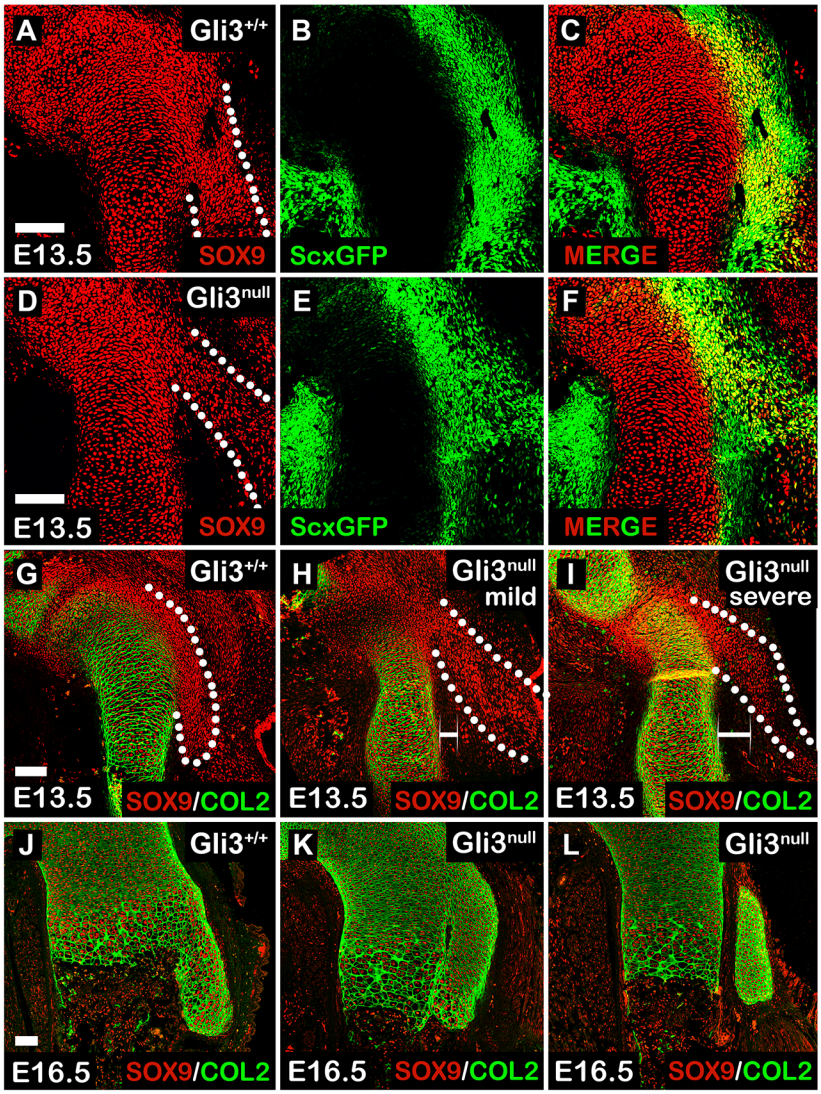

Fig. 3. Organization but not specification of *Sox9*$^{+}$/*Scx*$^{+}$ progenitors is regulated by *Gli3*. (A-F) Sagittal sections through the proximal humeri of E13.5 *Gli3;ScxGFP* transgenic embryos that were stained against SOX9. Although SOX9 and *Scx* co-expressing cells are observed in control and mutant embryos (C,F), their spatial organization is abnormal in *Gli3*^{null} mutants (A,D, dotted lines). (G-L) Sagittal sections through the proximal humeri of E13.5 (G-I) and E16.5 (J-L) *Gli3* KO and control embryos that were stained against SOX9 and COL2A1. At E13.5, spatial organization of deltoid tuberosity precursors is abnormal in mutants (G-I, dotted lines), displaying varying degrees of lateralization and distance from the humeral shaft (H,I, white brackets). In E16.5 mutants, aberrant deltoid tuberosity morphology ranges from aplasia (K) to detachment from the humeral shaft (L). Scale bars: 100 µm.

E12.0 (Fig. 5A). Next, we harvested E13.5 *Sox9-tdTomato*$^{+}$/*ScxGFP*$^{+}$ embryos and micro-dissected their forelimbs at the shoulder level, above the presumable deltoid tuberosity, and at flanking sides of the elbow (Fig. 5Bi,Bii). Finally, the dissected segments were collected into individual tubes, homogenized and then prospectively isolated by FACS (Fig. 5Biii). For each proximal and distal segment, we collected three biological repeats from three separate litters. Each sample contained 7-9% *Sox9-tdTomato*$^{+}$/*ScxGFP*$^{+}$ progenitors of total cell population, of which 10,000 cells were collected for transcriptome analysis (Fig. 5C). Further information regarding controls, gate settings and instrument configuration is found in Fig. 5D and in Materials and Methods.

Comparison between the transcriptomes of proximal and distal *Sox9-tdTomato*$^{+}$/*ScxGFP*$^{+}$ progenitors revealed 561 differentially expressed genes with at least two-fold change in expression levels between segments (Table S2). We further analyzed 40 of these genes that were considered most likely to be involved, based on the difference in expression levels, enrichment in relevant biological function and known roles in embryonic development (Fig. 5E,F). Notably, 16 of these 40 candidate genes (listed in Table 1) have previously been implicated in superstructure development, providing a strong validation for the effectiveness of our strategy.

Hoxa11, *Hoxd11* and *Pbx1* genes regionally regulate distal or proximal superstructure patterning

Our transcriptome analysis revealed that *Hoxa11* and *Hoxd11* were highly expressed in distal *Sox9-tdTomato*$^{+}$/*ScxGFP*$^{+}$ progenitors and scarcely expressed in proximal cells. Intriguingly, a previous study has demonstrated that a *Hoxa11/Hoxd11* compound mutation (*Hox11*^{aadd}) resulted in diverse distal forelimb abnormalities, such as the formation of a detached olecranon resembling a sesamoid bone, whereas the proximal limb segment, including the deltoid tuberosity, was not affected (Koyama et al., 2010). Nevertheless, the mechanism underlying the abnormal olecranon development remained to be elucidated. Therefore, we proceeded to study this process in *Hox11*^{aadd} mutant embryos.

To that end, we crossed double-heterozygous *Hox11*^{AaDd} mice and harvested embryos at E13.5 and E17.5 (Wellik and Capecchi, 2003). Examination of skeletal preparations from E17.5 control and mutant embryos validated the abnormal development of the olecranon (Fig. 6A,A′). Next, we validated the differential expression of *Hoxd11* by fluorescent *in situ* hybridization (FISH) assay on sagittal sections of E13.5 forelimbs. In agreement with our transcriptome analysis results, *Hoxd11* was highly expressed distally in proximity to the elbow, but scarcely expressed in proximal parts of the limb (Fig. 6B). Furthermore, *Hoxd11*

Development (2019) 146, dev167882. doi:10.1242/dev.167882

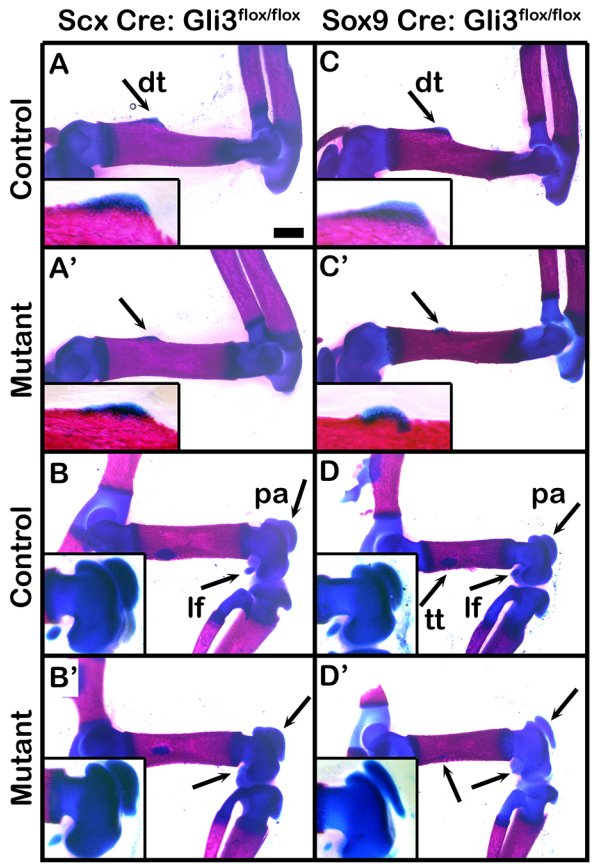

Fig. 4. Autonomous *Gli3* regulation has a mild effect on superstructure patterning. (A-D′) Skeletal preparations of E17.5 fore- and hindlimbs from tenocyte-specific *Scx-Cre;Gli3^{floxed}* cKO and control embryos (A-B′) and from chondrocyte-specific *Sox9-Cre;Gli3^{floxed}* cKO and control embryos (C-D′). Affected superstructures are indicated by black arrows. Insets show deltoid tuberosity or knee areas. dt, deltoid tuberosity; lf, lateral fabella; pa, patella; tt, third trochanter. Scale bar: 500 µm.

expression was downregulated in *Hox11^{aadd}* mutants (Fig. 6B′). The differential expression of *Hoxa11* at this stage has been previously demonstrated (Swinehart et al., 2013).

To study the regulatory roles of *Hoxa11* and *Hoxd11* in distal patterning of superstructure progenitors, we examined the patterning of the olecranon in control and mutant embryos. For this, we crossed double-heterozygous *Hox11^{AaDd}* mice and stained forelimb sections from E13.5 double-homozygous *Hox11^{aadd}* embryos using antibodies against SOX9 and COL2A1, such that the substructure cells were expected to be *Sox9^{+}/Col2a1^{+}* and the undifferentiated superstructure progenitors to be *Sox9^{+}/Col2a1^{-}*. Results showed that the olecranon progenitors failed to organize in the typical pattern observed in control limbs (Fig. 6C-E′). Specifically, the cells were scattered in a proximolateral direction away from the ulnar shaft (Fig. 6C,C′; dotted lines). Sections from E17.5 *Hox11^{aadd}* mutants illustrated that the olecranon precursors differentiated at a distance from the ulnar shaft, creating a distinct skeletal element resembling a sesamoid bone (Fig. 6F,F′). These results suggest that *Hoxa11* and *Hoxd11* are necessary for correct localization of the olecranon progenitors and, thus, for their patterning. Moreover, the proper patterning of superstructure progenitors on the proximal side supports our hypothesis that *Hoxa11* and *Hoxd11* act as regional distal regulators (Fig. S1A,A′).

Another promising candidate gene from our transcriptome analysis was *Pbx1*. In contrast to *Hoxa11* and *Hoxd11*, *Pbx1* was highly expressed in proximal *Sox9-tdTomato^{+}/ScxGFP^{+}* progenitors compared with distal cells. Indeed, *Pbx1^{null}* mutation has been shown to affect only proximal elements, such as the deltoid tuberosity, whereas the distal limb segment, including the olecranon, was not affected (Selleri et al., 2001). We therefore performed the same analysis on *Pbx1^{null};ScxGFP* mutants. After validation of the deltoid tuberosity phenotype in skeletal preparations of E15.0 control and mutant embryos (Fig. 6G,G′), we analyzed *Pbx1* expression by immunostaining sagittal sections of E13.5 forelimbs against PBX1 and COL2A1. In agreement with the transcriptome analysis results, PBX1 was highly expressed proximally in proximity to the deltoid tuberosity and was less prominent in the distal forelimb (Fig. 6H). As expected, PBX1 expression was completely ablated in *Pbx1^{null}* mutants (Fig. 6H′).

Next, forelimb sections from *Pbx1^{null};ScxGFP^{+}* E13.5 embryos were stained using antibodies against SOX9. As seen in Fig. 6I-K, the *Sox9^{+}/Scx^{+}* deltoid tuberosity precursors were specified in both control and mutant limbs; yet, in the mutant they were organized abnormally and scattered laterally. Finally, examination of sections immunostained against SOX9 and COL2A1 at E15.5 showed that in *Pbx1^{null}* mutants, the deltoid tuberosity precursors differentiated into a distinct sesamoid-like cartilaginous element parallel to the humeral shaft (Fig. 6L,L′). These results indicate that *Pbx1* is necessary for correct localization of the *Sox9^{+}/Scx^{+}* deltoid tuberosity precursors and, thus, for their patterning. Importantly, the patterning of superstructure progenitors at the distal region was independent of *Pbx1* regulation (Fig. S1B,B′).

Together, these results indicate that superstructure patterning is regulated regionally through early modulation of the spatial organization of *Sox9^{+}/Scx^{+}* progenitors by *Hoxa11*, *Hoxd11* and *Pbx1*.

Both *Pbx1* and *Pbx2* are involved in patterning of proximal superstructures

Pbx2 is a paralog of *Pbx1* that is expressed throughout the limb mesenchyme. Previously, it was shown that *Pbx1* and *Pbx2* act in a dosage-dependent manner during proximal limb development (Capellini, 2006). This led us to examine whether *Pbx2* co-regulates proximal superstructure patterning with *Pbx1*. To avoid early embryonic lethality, we ablated one allele of *Pbx2* on the background of a limb-specific knockout of *Pbx1* (*Prx1-Cre;Pbx1$^{fl/fl}$;Pbx2$^{+/-}$*) and compared the phenotype with both wild-type (*Prx1-Cre^{-};Pbx1$^{+/+}$;Pbx2$^{+/+}$*) and *Pbx1* cKO (*Prx1-Cre;Pbx1$^{fl/fl}$*) embryos (Ficara et al., 2008; Selleri et al., 2004). To this end, sections from E13.5, E15.5 and E16.5 control and mutant forelimbs were immunostained using antibodies against SOX9 and COL2A1 (Fig. 7A-C″). At E13.5, we observed abnormal patterning of deltoid tuberosity precursors in both *Prx1-Cre;Pbx1$^{fl/fl}$* and *Prx1-Cre;Pbx$^{fl/fl}$;Pbx2$^{+/-}$* mutant embryos. The precursors were laterally scattered (Fig. 7A′,A″), comparable to the deltoid tuberosity precursors of *Pbx1^{null}* limbs (Fig. 6I′). By E15.5, the deltoid tuberosity precursors of *Prx1-Cre;Pbx1$^{fl/fl}$* embryos had fully differentiated, whereas in *Prx1-Cre;Pbx1$^{fl/fl}$;Pbx2$^{+/-}$* we observed delayed differentiation (Fig. 7B-B″). Notably, in *Prx1-Cre;Pbx1$^{fl/fl}$* embryos the humerus-deltoid tuberosity boundary was populated by SOX9^{+} cells that had not been detected in *Prx1-Cre;Pbx1$^{fl/fl}$;Pbx2$^{+/-}$* embryos. Moreover, the gap between the humeral shaft and deltoid tuberosity precursors was roughly twice as large in *Prx1-Cre;Pbx1$^{fl/fl}$;Pbx2$^{+/-}$* limbs than in *Prx1-Cre;Pbx1$^{fl/fl}$* limbs. Finally, by E16.5, the deltoid tuberosity of *Prx1-Cre;Pbx1$^{fl/fl}$* embryos has attached to the humeral shaft, whereas the deltoid tuberosity of *Prx1-Cre;Pbx1$^{fl/fl}$;Pbx2$^{+/-}$* mutants remained

Development (2019) 146, dev167882. doi:10.1242/dev.167882

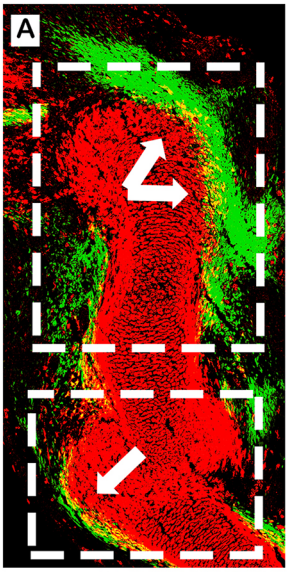

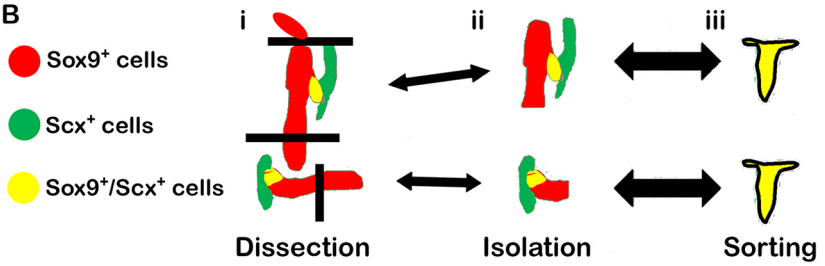

C

	# of Cells	% of Live cells
Total Cell Population	50000	100
Live Cells	33834	67.7
Single Cells	32186	95.1
Sox9-tdTomato^{hi}	180	0.66
ScxGFP^{hi}	3925	14.3
Sox9-tdTomato^{hi}/ ScxGFP^{hi}	2388	8.72
Negative cells	9700	35.4

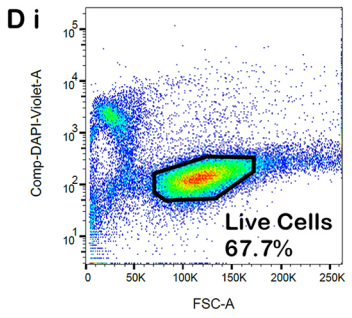

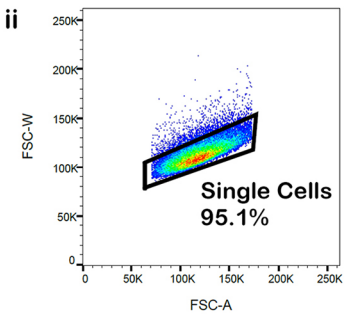

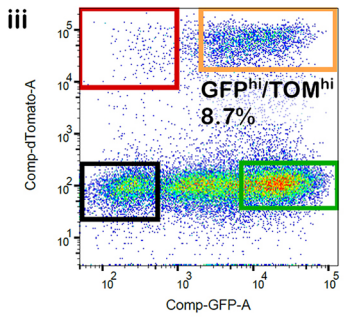

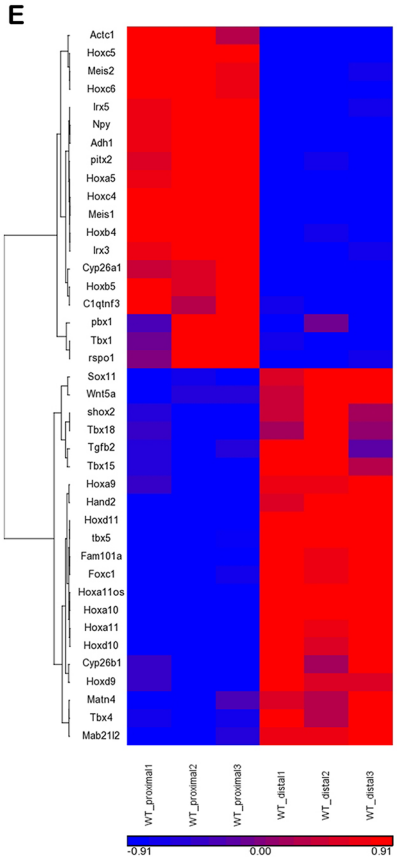

F

Top Diseases and Disorders		
Name	p-value range	#Molecules
Connective Tissue Disorders	1.74E-03 - 5.52E-25	23/40
Organismal Injury and Abnormalities	2.07E-03 - 5.52E-25	29/40
Skeletal and Muscular Disorders	2.07E-03 - 5.52E-25	23/40
Developmental Disorder	2.07E-03 - 3.94E-17	27/40
Top Molecular and Cellular Functions		
Name	p-value range	#Molecules
Gene Expression	1.24E-05 - 2.02E-12	21/40
Cellular Development	2.07E-03 - 2.08E-08	24/40
Cellular Growth and Proliferation	2.07E-03 - 2.08E-08	20/40
Cell Morphology	2.07E-03 - 5.59E-07	16/40
Top Physiological System Development and Function		
Name	p-value range	#Molecules
Embryonic Development	2.07E-03 - 3.88E-29	35/40
Skeletal and Muscular System Development and Function	2.07E-03 - 3.88E-29	28/40
Tissue Morphology	2.07E-03 - 1.51E-23	30/40
Connective Tissue Development and Function	2.07E-03 - 4.83E-22	27/40

Fig. 5. See next page for legend.

Development (2019) 146, dev167882. doi:10.1242/dev.167882

Fig. 5. Comparative transcriptomic analysis highlights regional regulation of superstructure patterning. (A) Sagittal section through the forelimb of E13.5 *Sox9-CreER^{tdTomato};Scx-GFP* transgenic reporter embryo following tamoxifen administration at E12.0. *Sox9* and *Scx* co-expressing cells are indicated by white arrows. Dashed white rectangles indicate the proximal and distal regions of interest that were dissected for FACS and transcriptome analysis. (B) Schematics of sample preparation. Labeled forelimbs were dissected (i), the proximal and distal segment cells were isolated (ii) and then sorted independently (iii). (C) A table summarizing cell type distribution among 50,000 collected and FACS-sorted cells. The number and percentage of *Sox9-tdTomato*$^+$/*ScxGFP*$^+$ progenitors are indicated by a black arrow. (D) Illustrations of control and gating settings. (i) Live cells were controlled for by DAPI staining. (ii) Single cells were gated according to droplet area (FSC-A) versus width (FSC-W). (iii) Gating settings for *Sox9-tdTomato*$^+$/*ScxGFP*$^+$ progenitors resulted in collection of 7-9% of the total living single-cell population (orange rectangle). Colored rectangles indicate populations as listed in C. (E) Heat map showing the clustering of 40 of the most differentially expressed genes between proximal and distal *Sox9-tdTomato*$^+$/*ScxGFP*$^+$ progenitors. (F) Using Ingenuity software, these genes were annotated and found to be biologically relevant to limb development and tissue morphology.

separated (Fig. 7C-C″), as in *Pbx1^{null}* mutants (Fig. 6L′). These diverging morphologies were further validated by skeletal preparations made of limbs taken from each mutants (Fig. 7D-D″). Taken together, these results suggest that PBX genes act together in regulating the patterning of proximal superstructures, possibly by regulating the level of lateralization in a dose-dependent manner.

Interaction between global and regional genetic programs fine-tunes patterning of superstructures

The finding that superstructure patterning can be regulated both globally and regionally led us to hypothesize that these two programs interact with one another. To examine this possibility, we produced a compound mutant mouse carrying limb-specific knockout of *Pbx1* and *Gli3*. Specifically, on the background of a limb-specific knockout of *Pbx1* (*Prx1-Cre;Pbx1$^{fl/fl}$*) we ablated either one or two alleles of *Gli3* (*Prx1-Cre;Pbx1$^{fl/fl}$;Gli3$^{fl/+}$* or *Prx1-Cre;Pbx1$^{fl/fl}$;Gli3$^{fl/fl}$*, respectively). Then, sections from E13.5 and E16.5 control and mutant forelimbs were immunostained using antibodies against SOX9 and COL2A1 (Fig. 8A-B″). At E13.5, deltoid tuberosity precursors in the *Prx1-Cre;Pbx1$^{fl/fl}$;Gli3$^{fl/fl}$* embryos were laterally scattered and noticeably less condensed than in *Prx1-Cre;Pbx1$^{fl/fl}$;Gli3$^{fl/+}$* embryos (Fig. 8A-A″). The phenotypic difference between genotypes became more pronounced by E16.5. Whereas ablation of a single *Gli3* allele resulted in a dysplastic deltoid tuberosity that was attached to the humeral shaft, ablation of both alleles resulted in a detached deltoid tuberosity (Fig. 8B-B″). These diverging morphologies were further validated by skeletal preparations of limbs from each mutant group (Fig. 8C-C″). Importantly, whereas individual limb-specific knockout of either *Prx1-Cre;Gli3$^{fl/fl}$* (data not shown) or *Prx1-Cre;Pbx1$^{fl/fl}$* (Fig. 7D′) resulted in dysplastic deltoid tuberosity, the compound *Prx1-Cre;Pbx1$^{fl/fl}$;Gli3$^{fl/fl}$* double knockout mutant displayed a detached deltoid tuberosity, as in both *Gli3^{null}* (Fig. 2G) and *Pbx1^{null}* (Fig. 6G′) embryos. These results suggest that, similar to the compound *Pbx1/Pbx2* mutation, genetic interactions also occurred between *Pbx1* and *Gli3* in a dose-dependent manner, highlighting the possibility of interactions between the global and regional regulatory programs.

The mechanism underlying the abnormal superstructure development

The abnormal superstructure development we observe in the different mutant mouse models could be the result of several possible mechanisms that affect the *Sox9*$^+$/*Scx*$^+$ progenitors, including patterning, proliferation, differentiation and cell death. Having already demonstrated abnormal patterning of the *Sox9*$^+$/*Scx*$^+$ progenitors in the different mutants, we next sought to study whether proliferation rate contributed to the observed phenotype. To this end, we analyzed incorporation of 5-bromo-2-deoxyuridine (BrdU) into *Sox9*$^+$/*Scx*$^+$ cells, focusing on the hypoplastic deltoid tuberosity. *Gli3* and *Prx1-Cre;Pbx1;Pbx2* pregnant mice were injected subcutaneously with BrdU. Incorporation of BrdU was allowed for a period of 2 h, after which the pregnant mice were sacrificed. Incorporated BrdU was detected by immunostaining using antibodies against BrdU and SOX9 on sections taken from E13.5 *Gli3* and *Prx1-Cre;Pbx1;Pbx2* control and mutant forelimbs. Next, the total SOX9$^+$ and SOX9$^+$/BrdU$^+$ cells were counted in the region of the greater and deltoid tuberosities and the fraction of proliferating cells was calculated for both control and mutant embryos (Fig. S2). Our results showed that in *Gli3* mutants, the center of proliferation appeared to shift inwards from the lateral side of the superstructures to the main shaft (Fig. 9A′,B′; yellow arrows demarcate center of proliferation). However, quantification showed no significant difference in the fraction of proliferating cells. In contrast, we observed a mild but significant reduction of proliferating cells in both *Prx1-Cre;Pbx1^{floxed}* and *Prx1-Cre;Pbx1^{floxed};Pbx2^{het}* mutant embryos (Fig. 9D′,E′) compared with control embryos (Fig. 9C′) (Fig. S2).

Table 1. Genes previously implicated in regional regulation of superstructure patterning

Gene symbol	Gene name	Fold change (proximal/distal)	Reference
Pitx2	Paired like homeodomain 2	−3.40	Holmberg et al., 2008
Meis1	Meis homeobox 1	−2.23	Mercader et al., 2009
Irx3	Iroquois homeobox 3	−1.60	Li et al., 2014
Irx5	Iroquois homeobox 5	−1.07	Cain et al., 2016
Pbx1	PBX homeobox 1	−0.53	Selleri et al., 2001
Wnt5a	Wnt family member 5A	+0.87	Yang et al., 2003
Shox2	Short stature homeobox 2	+1.01	Neufeld et al., 2014
Hoxa9	Homeobox A9	+1.03	Xu and Wellik, 2011
Cyp26B1	Cytochrome P450 family 26 subfamily B member 1	+1.59	Yashiro et al., 2004
Tbx5	T-box 5	+1.61	Hasson et al., 2007
Hoxd9	Homeobox D9	+2.63	Xu and Wellik, 2011
Hand2	Heart and neural crest derivatives expressed 2	+2.74	Galli et al., 2010
Hoxa10	Homeobox A10	+2.85	Wellik and Capecchi, 2003
Hoxd10	Homeobox D10	+3.71	Wellik and Capecchi, 2003
Hoxa11	Homeobox A11	+3.91	Boulet and Capecchi, 2004
Hoxd11	Homeobox D11	+4.01	Gross et al., 2012

Development (2019) 146, dev167882. doi:10.1242/dev.167882

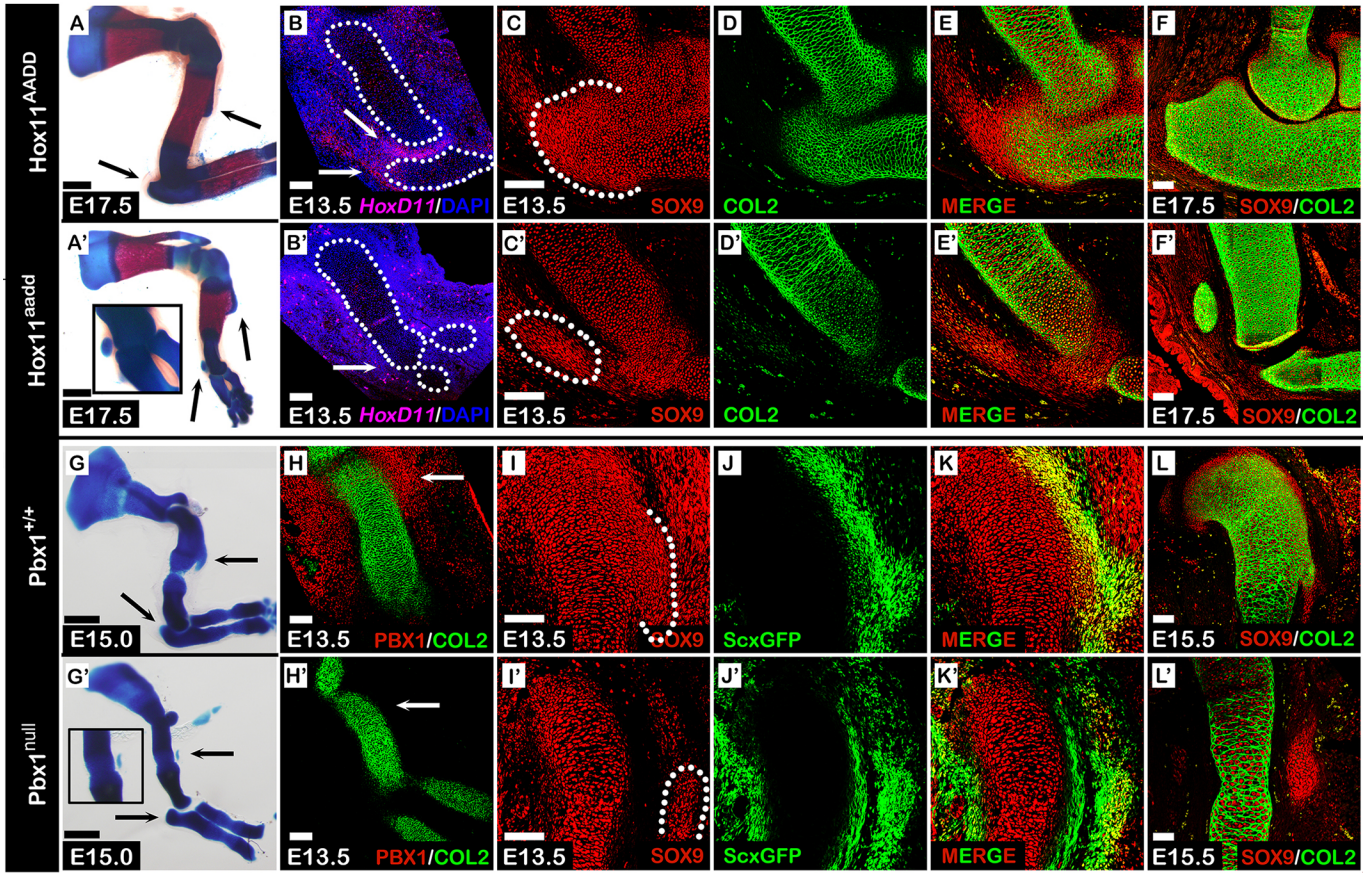

Fig. 6. Distal and proximal superstructure patterning is regulated by *Hoxa11*, *Hoxd11* and *Pbx1*. (A-F′) *Hoxa11* and *Hoxd11* regionally regulate patterning of the distal olecranon. (A,A′) Skeletal preparations of E17.5 forelimbs from compound *Hoxa11* and *Hoxd11* mutant and control embryos. Distal olecranon but not proximal deltoid tuberosity developed abnormally in *Hox11*^{aadd} mutant forelimbs (black arrows and inset). (B,B′) Fluorescent *in situ* hybridization for *Hoxd11* in forelimb sections shows that at E13.5, *Hoxd11* is distally expressed in the elbow region (B, white arrows). Expression of *Hoxd11* was downregulated in *Hox11*^{aadd} mutant forelimbs (B′). Long bones are demarcated by dotted lines. (C-F′) Sagittal sections through the elbow of E13.5 (C-E′) and E17.5 (F,F′) *Hox11*^{aadd} compound mutant and control embryos that were stained against SOX9 and COL2A1. At E13.5, spatial organization of olecranon precursors is abnormal (C,C′). By E17.5, the developing olecranon of mutant embryos has detached from the ulnar shaft (F,F′). (G-L′) *Pbx1* regionally regulates patterning of the proximal deltoid tuberosity. (G,G′) Skeletal preparations of E15.0 forelimbs from *Pbx1*-null and control embryos. Proximal deltoid tuberosity but not distal olecranon developed abnormally in *Pbx1* mutant forelimbs (black arrows and inset). (H,H′) Staining against PBX1 and COL2A1 in forelimb sections shows that at E13.5, *Pbx1* is proximally expressed at the shoulder region (H, white arrows). Expression of *Pbx1* was downregulated in *Pbx1*^{null} mutant forelimbs (H′). (I-K′) Sagittal sections through the proximal humeri of E13.5 *Pbx1;ScxGFP* transgenic embryos that were stained against SOX9. Although SOX9 and *Scx* co-expressing cells are observed in control and mutant embryos (K,K′), their spatial organization was abnormal in *Pbx1*^{null} mutants (I,I′). (L,L′) Sagittal sections through the proximal humeri of E15.5 *Pbx1* mutant and control embryos that were stained against SOX9 and COL2A1. At E15.5, the deltoid tuberosity of mutant embryos is detached from the humeral shaft (L,L′). Scale bars: 500 µm (skeletal preparations); 100 µm (sections).

The detached deltoid tuberosity could be the consequence of apoptosis. To examine the possible involvement of cell death in this phenotype, we performed a terminal deoxynucleotidyl transferase dUTP nick end labeling (TUNEL) assay on sections taken from E13.5 *Gli3* and *Prx1-Cre;Pbx1;Pbx2* control and mutant forelimbs. As a control, we examined the interdigital space, which undergoes massive cell death at E13.5 (Fig. 9F, inset). Results showed no cell death within the superstructure precursors in either control or mutant embryos (Fig. 9F-J; superstructures are demarcated by dotted lines).

Previously, we showed that BMP4 is necessary for the differentiation of superstructure progenitors (Blitz et al., 2009). To address the possibility that BMP signaling is reduced in our mutants, we examined the activation of SMAD1/5/8 (Retting et al., 2009) in the *Sox9*$^{+}$/*Scx*$^{+}$ progenitors. Sections taken from E13.5 *Gli3* and *Prx1-Cre;Pbx1;Pbx2* control and mutant forelimbs that were immunostained using antibodies against pSMAD1/5/8 and COL2A1 revealed different patterns of pSmad1/5/8 activity in control and mutant embryos (Fig. 9K-O), yet the abnormal patterns correlated with the mispatterning of the *Sox9*$^{+}$/*Scx*$^{+}$ progenitors in these mutants. This finding suggests that the aberrant Smad activation is secondary to the progenitor mispatterning. Overall, we concluded that although cell death did not contribute to the observed phenotypes, reduction in cell proliferation might have had some effect.

DISCUSSION

The musculoskeletal system acts as a system of levers and pulleys to create locomotion. Thus, one way to achieve variation in locomotor strategies is by changing the location of the connection between lever and pulley. Shifting the position of a bone superstructure, to which a muscle is connected by a tendon, along the bone shaft modifies the pulling force vector of that given muscle and, thereby, facilitates different types of locomotive capabilities. Variations in the positioning of superstructures and their effect on locomotion have been well documented (Archer et al., 2011; Milne and O'Higgins,

Development (2019) 146, dev167882. doi:10.1242/dev.167882

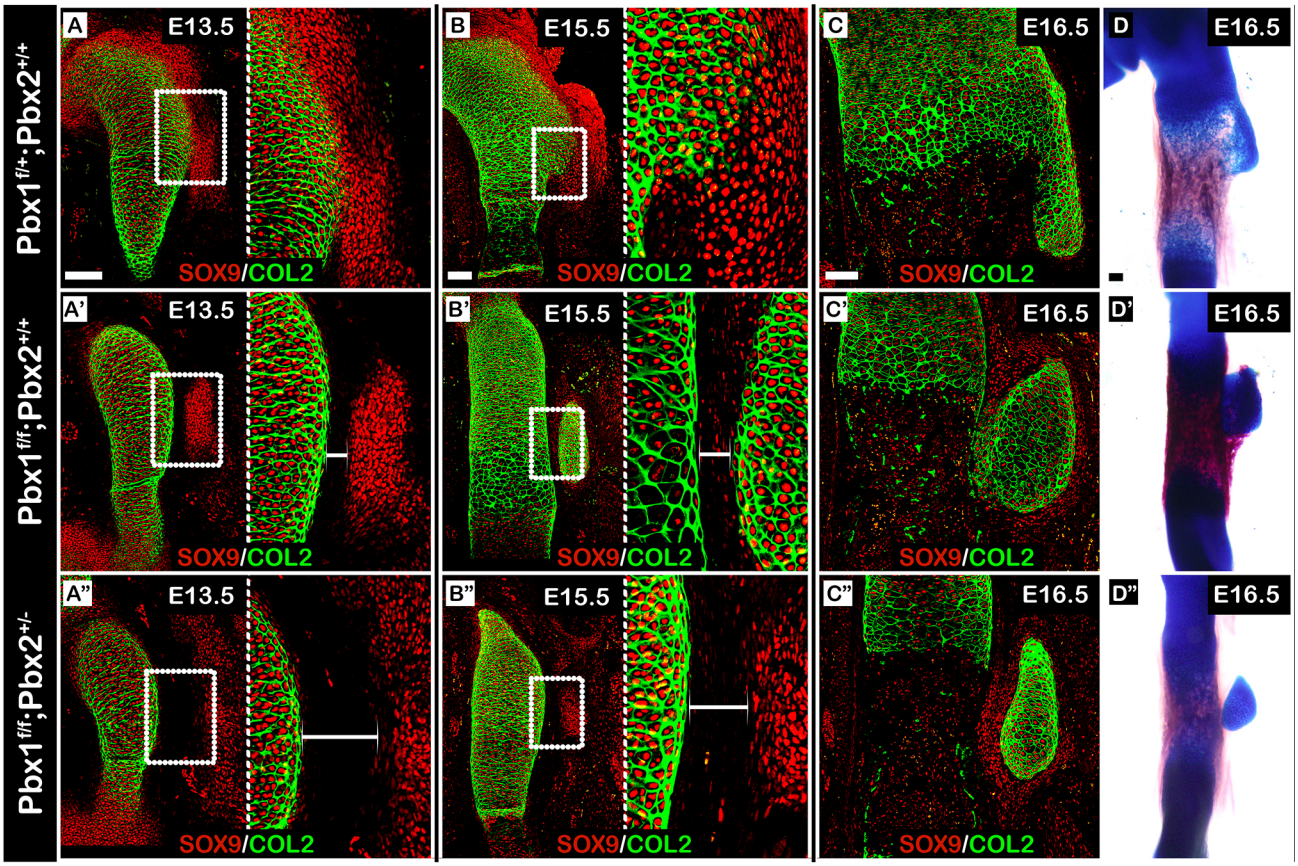

Fig. 7. *Pbx1* and *Pbx2* coordinately regulate the patterning of proximal superstructures. (A-C″) Sagittal sections through the proximal humeri of E13.5 (A-A″), E15.5 (B-B″) and E16.5 (C-C″) limbs from control (A-C), *Prx1-Cre;Pbx1*^{floxed} (B-B″) or *Prx1-Cre;Pbx1*^{floxed}*;Pbx2*^{het} (C-C″) embryos that were stained against SOX9 and COL2A1. In A-B″, the right side of the panel is an enlargement of the humerus-deltoid tuberosity boundary region demarcated by a white rectangle on the left. At E13.5, spatial organization of deltoid tuberosity precursors in both mutants was abnormal (A′,A″) as deltoid tuberosity precursors were scattered laterally away from the humeral shaft. The gap between the humeral shaft and deltoid tuberosity precursors was twice as large in *Prx1-Cre;Pbx1*^{floxed}*; Pbx2*^{het} mutants than in *Prx1-Cre;Pbx1*^{floxed} mutants (A′,A″, white brackets). At E15.5, whereas cells at the humerus- deltoid tuberosity boundary of *Prx1-Cre; Pbx1*^{floxed} mutants began to express high levels of SOX9, such expression was not observed in *Prx1-Cre;Pbx1*^{floxed}*;Pbx2*^{het} mutants. Moreover, the difference in boundary region size remained consistent (B,B′, white brackets). At E16.5, deltoid tuberosity morphology ranged from attached but aplastic deltoid tuberosity in *Prx1-Cre;Pbx1*^{floxed} mutants (C′) to a detached deltoid tuberosity in *Prx1-Cre;Pbx1*^{floxed}*;Pbx2*^{het} mutants (C″). (D-D″) Skeletal preparations of E16.5 forelimbs further validate these diverging morphologies. Scale bars: 100 µm.

2012; Polly, 2007; Salton and Sargis, 2008, 2009). However, the mechanism that produces these variations was unknown.

An early step in the development of endochondral bones is mesenchymal condensation and the formation of the cartilaginous template that prefigures the future bone. Here, we identify components of the genetic program that regulate the subsequent step of this process, namely the patterning and condensation of superstructure precursors. Moreover, we demonstrate that the mechanism of superstructure patterning involves both global and regional modules, highlighting the modularity in long bone development. Specifically, by combining comparative transcriptomic analysis with cross-reference to existing literature, we identified a list of candidate genes that might be involved in this genetic program. Further analysis of several of these candidate genes, namely, *Gli3*, *Pbx1*, *Pbx2*, *Hoxa11* and *Hoxd11*, established their involvement in regulating superstructure patterning. Importantly, *Gli3* perturbation affected superstructures throughout different parts of the limb skeleton, whereas mutations in *Pbx1* and *Pbx2* or in *Hoxa11* and *Hoxd11* affected either proximal or distal superstructures, respectively. Interestingly, we found that the global and regional components of the genetic program are interconnected, as compound mutations of the proximal regulator *Pbx1* and the global regulator *Gli3* led to increased phenotype severity, compared with mutations in either gene alone.

In addition to these genes, our transcriptomic analysis identified 12 more candidate genes that were reportedly involved in long bone development. Interestingly, many of these genes regulate either proximal or distal limb segments, or alternatively, establish the proximodistal axis itself. For example, we identified additional HOX genes, such as *Hoxa9*, *Hoxd9*, *Hoxa10* and *Hoxd10*, which were shown to regulate the patterning of proximal superstructures, such as the deltoid tuberosity (Wellik and Capecchi, 2003; Xu and Wellik, 2011). Other candidate genes, such as *Shox2* or *Meis1*, operate locally either as downstream effectors of HOX genes (Neufeld et al., 2014) or as co-factors of proximal regulators, such as *Pbx1* (Mercader et al., 2009), respectively. We also identified genes that control the formation of the proximodistal axis, such as *Cyp26B1*, which modulates the levels of retinoic acid (Yashiro et al., 2004) or *Irx3*, *Irx5* and *Hand2*, which modulate the activity of the *Shh*/*Gli3* signaling pathway (Galli et al., 2010; Li et al., 2014). Together, these reports further support the modular model for superstructure patterning and suggest the involvement of at least two hierarchical programs in this process. Higher is the program that governs the establishment of the proximodistal axis and, further

Development (2019) 146, dev167882. doi:10.1242/dev.167882

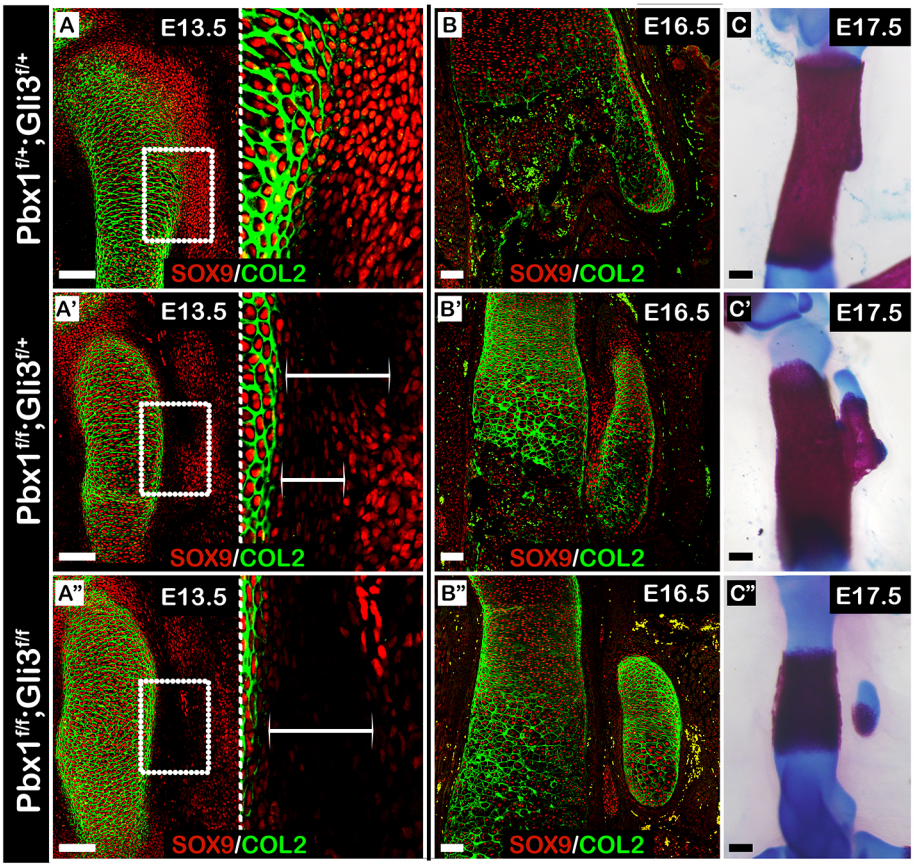

Fig. 8. Coordinated regulation by *Pbx1* and *Gli3* highlights interaction between global and regional genetic programs. (A-B″) Sagittal sections through the proximal humeri of E13.5 (A-A″) and E16.5 (B-B″) limbs from control (A,B), *Prx1-Cre;Pbx1*^{floxed};*Gli3*$^{fl/+}$ (A′,B′) or *Prx1-Cre;Pbx1*^{floxed};*Gli3*^{floxed} (A″,B″) embryos that were stained against SOX9 and COL2A1. (C-C″) Skeletal preparations of E17.5 forelimbs from control (C), *Prx1-Cre;Pbx1*^{floxed};*Gli3*$^{fl/+}$ (C′) or *Prx1-Cre;Pbx1*^{floxed};*Gli3*^{floxed} (C″) embryos. In A-A″, the right side of the panel is an enlargement of the humerus-deltoid tuberosity boundary region demarcated by a white rectangle on the left. At E13.5, spatial organization of deltoid tuberosity precursors in both mutants was abnormal (A′,A″) as deltoid tuberosity precursors were scattered laterally away from the humeral shaft. The gap between the humeral shaft and deltoid tuberosity precursors was twice as large in *Prx1-Cre;Pbx1*^{floxed};*Gli3*^{floxed} mutants than in *Prx1-Cre;Pbx1*^{floxed};*Gli3*$^{fl/+}$ mutants (A′,A″, white brackets). At E16.5, whereas cells at the humerus-deltoid tuberosity boundary of *Prx1-Cre;Pbx1*^{floxed};*Gli3*$^{fl/+}$ mutants began to express high levels of SOX9, such expression was not observed in *Prx1-Cre;Pbx1*^{floxed};*Gli3*^{floxed} mutants. Moreover, the difference in boundary region size remained consistent (B′,B″). At E17.5, deltoid tuberosity morphology ranged from attached but aplastic deltoid tuberosity in *Prx1-Cre;Pbx1*^{floxed};*Gli3*$^{fl/+}$ mutants (C′) to a detached deltoid tuberosity in *Prx1-Cre;Pbx1*^{floxed};*Gli3*^{floxed} mutants (C″). Scale bars: 200 µm (skeletal preparations); 100 µm (sections).

downstream, local programs adjust the development of each individual segment. Finally, whereas our transcriptomic analysis was designed to highlight differentially expressed genes along the proximodistal axis, it lacked information regarding globally expressed genes, which could potentially regulate superstructure patterning, such as *Gli3*, which was expressed ubiquitously in both proximal and distal *Sox9*$^{+}$/*Scx*$^{+}$ progenitors. Additional evidence for the existence of other global regulatory genes is given by a recent report demonstrating that *Tbx3* globally regulates patterning of forelimb superstructures, namely the greater and deltoid tuberosity and olecranon (Colasanto et al., 2016).

Although our work sheds light on the genetic mechanism that regulates superstructure patterning, the cellular mechanism underlying the patterning process is still missing. A clue for its nature is given by the observations that in *Gli3*, *Pbx* and *Hox11* mutant embryos, superstructure precursors spread abnormally away from the developing bone substructure and display delayed differentiation. This may imply the existence of a mechanism controlling the migration of *Sox9*$^{+}$/*Scx*$^{+}$ progenitors to a specific condensation site. Once this program is perturbed, cells migrate to the wrong site, where they form an abnormal bony element. Alternatively, it is possible that *Sox9*$^{+}$/*Scx*$^{+}$ chondroprogenitors are specified from selected cells already present at the designated superstructure locations. In that case, the mechanism would involve activation of a chondrogenic program in specific cell subpopulations by extrinsic or intrinsic signals at specific spatiotemporal positions. In either scenario, it appears that the mechanism that decides where superstructure development should take place involves the *Gli3*, *Pbx* and *Hox* genes. Our finding that ablation of *Gli3* specifically in *Sox9*$^{+}$ and/or *Scx*$^{+}$ cell lineage resulted in hypoplasia of selected superstructures clearly suggests that *Gli3* regulates the *Sox9*$^{+}$/*Scx*$^{+}$ progenitors autonomously. However, the differences we observed in the severity of the phenotype between the *Gli3*-null and the different conditional alleles may suggest a non-autonomous contribution as well. An alternative explanation for the differences in severity is differences in efficiency between the various Cre lines in targeting the *Gli3* locus.

A previous work in which the expression of both *Shh* and *Gli3* was blocked proposed that the function of *Shh* and *Gli3* in limb skeletal patterning is limited to refining autopodial morphology (Litingtung et al., 2002). Our work clearly expands the involvement of *Gli3* in skeletal patterning by demonstrating its role as a global regulator of superstructure patterning. Interestingly, both *Shh* loss of function and *Shh/Gli3* double knockout resulted in apparently normal deltoid tuberosity, suggesting that the effect of *Gli3*, at least in the proximal domain of the limb, is independent of *Shh*.

The patterning of superstructures involves control over their size. Our finding of reduced progenitor cell proliferation in *Prx1-Cre;Pbx1*$^{fl/fl}$ and *Prx1-Cre;Pbx1*$^{fl/fl}$;*Pbx2*$^{+/-}$ mutant embryos might suggest that the genetic program regulates superstructure morphology by coordinating patterning and cell proliferation. In contrast, we present evidence that size control does not involve apoptosis of *Sox9*$^{+}$/*Scx*$^{+}$ progenitors.

Another level of coordination that is required is between the skeleton and the musculature. Interestingly, several reports have demonstrated that mispatterning of specific muscles is coupled with aberrant superstructures. For example, ablation of *Tbx3* results in abnormal patterning of stylopod musculature, which attaches to dysplastic olecranon and deltoid tuberosity (Colasanto et al., 2016), whereas in *Hox11*^{Aadd} or *Hox11*^{aaDd} compound mutants, abnormal patterning of zeugopod musculature is accompanied by abnormal

Development (2019) 146, dev167882. doi:10.1242/dev.167882

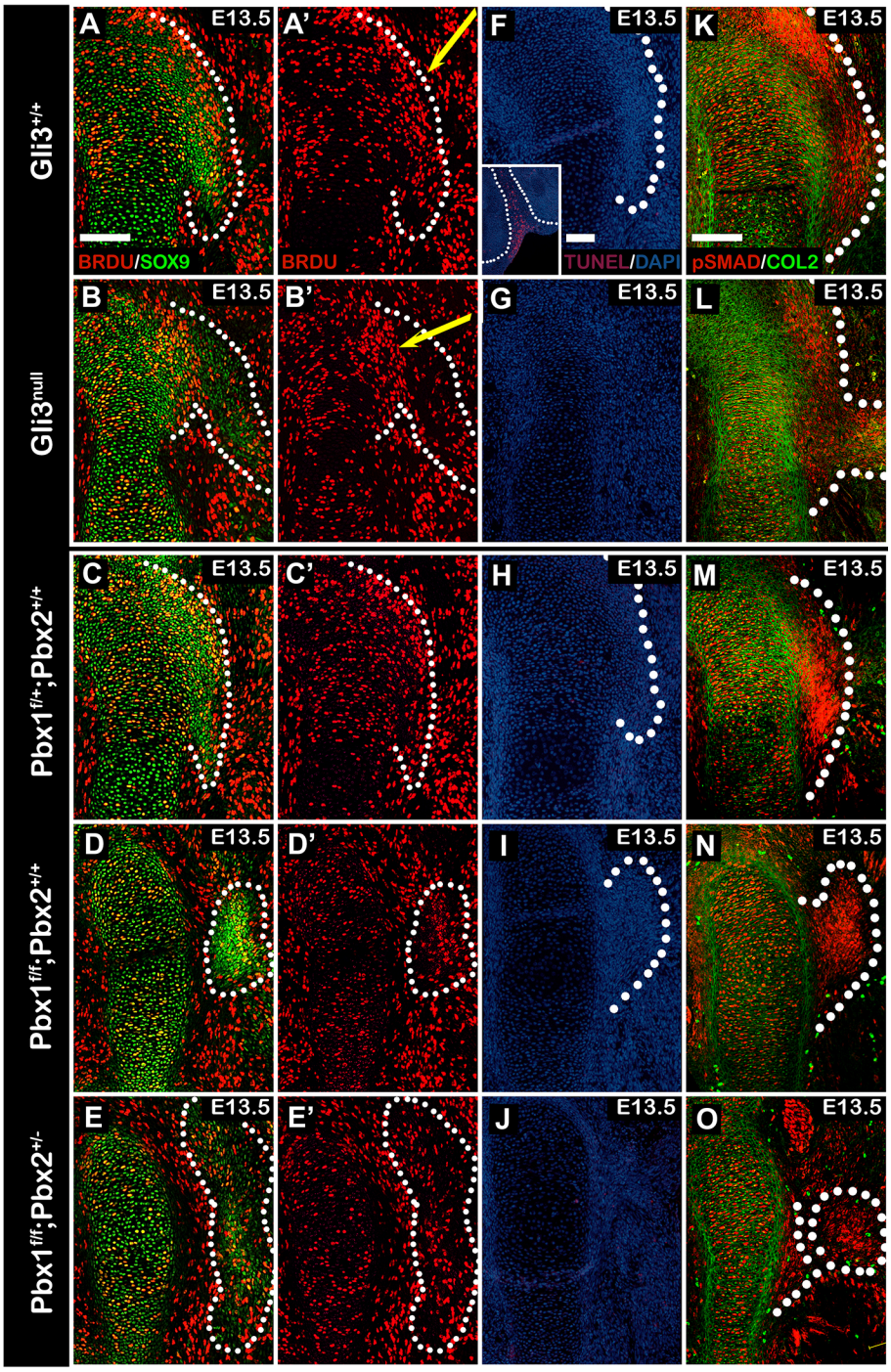

Fig. 9. Superstructure size and shape is independent of proliferation, differentiation or apoptosis. (A-O) Sagittal sections through the proximal humeri of E13.5 *Gli3* control (A,A′,F,K) and mutant (B,B′,G,L) embryos or from control (C,C′,H,M), *Prx1-Cre;Pbx1*^{floxed} (D,D′, I,N) or *Prx1-Cre;Pbx1*^{floxed}*;Pbx2*^{het} (E,E′,J,O) embryos. (A-E′) BrdU staining was performed to highlight proliferating cells within the superstructure precursors (demarcated by dotted lines). No reduction in proliferating cells was observed in *Gli3* mutants; however, the center of proliferation appeared to shift from the lateral face of the superstructures in control embryos to the main shaft of the mutant embryos (A′,B′; yellow arrows demarcate center of proliferation). In *Prx1-Cre; Pbx1*^{floxed} (D,D′) and *Prx1-Cre;Pbx1*^{floxed}*;Pbx2*^{het} (E,E′) mutant embryos, we observed a mild reduction of proliferating cells in comparison with the control embryos (C,C′). (F-J) TUNEL staining was performed to highlight apoptotic cells within the superstructure precursors (demarcated by dotted lines). No cell death within the superstructure precursors was noticed in either control or mutant embryos. The interdigital space, which undergoes massive cell death at E13.5, was used as control for the staining (F, inset). (K-O) To highlight differentiating cells within the superstructure precursors (demarcated by dotted lines), we performed immunostaining for pSMAD1/5 and counterstained for COL2A1. The results show high pSMAD1/5 activity within all superstructure precursors indicating normal differentiation in both control and mutant embryos. Scale bars: 100 µm.

olecranon patterning (Swinehart et al., 2013). Taken together, these results strongly suggest that muscle and superstructure patterning may be regulated in a coordinated manner.

Previously, we reported that sesamoid bones, which are small auxiliary bones that are highly variant in anatomical location, size and number, also originate from Sox9- and Scx-positive precursors (Eyal et al., 2015; Eyal et al., 2019). Interestingly, we demonstrated that the Sox9- and Scx-positive precursors of some sesamoid bones, such as the lateral fabella, were patterned such that they developed away from the long bone substructure (Eyal et al., 2019). Those results are in line with our current evidence showing the formation of sesamoid-like bones following perturbation in either Gli3, PBX or Hox11 genes. Moreover, they further highlight the degree of plasticity stemming from the modular model, which offers an evolutionary mechanism to induce not only local variations in bone morphology by patterning the superstructures, but also formation of new auxiliary bones without having to rewrite the entire skeletogenic program. We therefore propose that bone superstructures and sesamoid bones be placed under one category of cartilage elements that share a common origin and developmental program.

To conclude, our results provide insight into the formation, patterning and development of long bone superstructures and their impact on bone morphology. Furthermore, they provide strong evidence in support of the modular model of skeletogenesis and demonstrate the level of modularity during long bone morphogenesis in terms of cellular origins, genetic regulation, morphology and skeletal

Development (2019) 146, dev167882. doi:10.1242/dev.167882

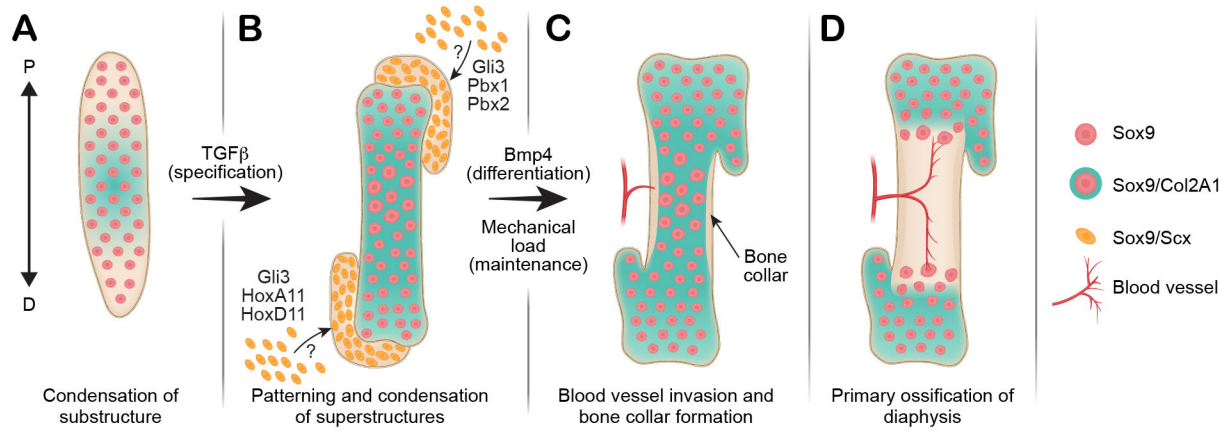

Fig. 10. A modular model for long bone development and superstructure patterning. (A) Superstructure initiation is preceded by formation of the cartilaginous substructures derived from primary *Sox9*$^{+}$ progenitors. (B) Subsequent to substructure differentiation, a secondary wave of *de novo* specification produces *Sox9*$^{+}$/*Scx*$^{+}$ superstructure progenitors. This second specification wave occurs in juxtaposition to the substructure at different time points during embryogenesis and is regulated by the TGFβ signaling pathway. The initial spatial patterning of superstructure progenitors is regulated by both global and regional molecular players, such as *Gli3* or *Pbx* and *Hox* genes, respectively. (C) Following specification, patterning and condensation of the superstructure precursors, they differentiate and become integral to the substructure anlagen, thus producing a complex three-dimensional cartilaginous template that is unique to each long bone. Differentiation of the superstructure is regulated by intrinsic BMP4 signaling and extrinsic mechanical stimuli. (D) Finally, ossification of the substructure, and later of the superstructures, will give rise to the morphology of the mature long bone. D, distal; P, proximal.

assembly of superstructures, namely their ability to attach or detach from the substructure. Specifically, we show that whereas *Sox9*$^{+}$ progenitors establish the bone substructure (Fig. 10A), superstructure anlagen are formed and assembled modularly onto the substructure by *Sox9*$^{+}$/*Scx*$^{+}$ progenitors (Fig. 10B). We show that these unique *Sox9*$^{+}$/*Scx*$^{+}$ progenitors contribute not only to bone eminences but also to various condyles and sesamoid bones and that their patterning involves both global and regional regulatory modules that include *Gli3*, *Pbx* and *Hox* genes (Fig. 10B). Following their specification and patterning, these superstructures differentiate and become integral to the developing long bones (Fig. 10C,D). Importantly, by performing a comparative transcriptomic analysis, we were able to highlight additional candidate genes that may be implicated in superstructure patterning. Further studies of these molecular players will provide a better understanding of the regulatory network at play in superstructure formation and long bone morphogenesis.

MATERIALS AND METHODS

Animals

All experiments involving mice were approved by the Institutional Animal Care and Use Committee (IACUC) of the Weizmann Institute. For all timed pregnancies, plug date was defined as E0.5. For harvesting of embryos, timed-pregnant females were euthanized by cervical dislocation. The gravid uterus was dissected out and suspended in a bath of cold PBS and the embryos were harvested after removal of the placenta. Tail genomic DNA was used for genotyping by PCR. All experiments were performed in at least three biological repeats, i.e. on three embryos from separate litters.

Sox9-CreER^{T2} mice (Soeda et al., 2010) were received from the laboratory of Haruhiko Akiyama, Kyoto University, Kyoto, Japan. *ScxGFP*,*Scx-Cre* and *Sox9-Cre* transgenic mice were obtained from Ronen Schweitzer, Shriners Hospital for Children Research Division, Portland, OR, USA.

The generation of *Col2A1-CreER*^{T2} (Nakamura et al., 2006), *Sox9-CreER*^{T2} (Soeda et al., 2010), *ScxGFP* (Pryce et al., 2007), *Gli3*^{null} (Johnson, 1967), *Prx1-Cre* (Logan et al., 2002), floxed-*Gli3* (Blaess et al., 2008), *Pbx1*^{null} (Selleri et al., 2001), floxed-*Pbx1* (Ficara et al., 2008), *Pbx2*^{null} (Selleri et al., 2004), *Hox-a11*^{null} (Hsieh-Li et al., 1995), *Hox-d11*^{null} (Davis and Capecchi, 1994) and *Rosa26-tdTomato* (Madisen et al., 2010) mice has been described previously.

To create *Gli3*, *Hox11*^{aadd} and *Pbx1* mutant mice, animals heterozygous for the mutations were crossed; heterozygous embryos were used as a control. To create *Prx1-Gli3* or *Prx1-Pbx1* mutant mice, floxed-*Gli3* or floxed-*Pbx1* mice were mated with *Prx1-Cre-Gli3* or *Prx1-Cre-Pbx1*, respectively. To create *Sox9-Gli3* or *Scx-Gli3* mutant mice, floxed-*Gli3* mice were mated with *Sox9-Cre-Gli3* or *Scx-Cre-Gli3*, respectively. To create *Prx1-Pbx1*^{flox}*-Pbx2*$^{+/-}$ mutant mice, floxed-*Pbx1-Pbx2*$^{+/-}$ mice were mated with *Prx1-Cre-Pbx1*^{flox} mutant mice. To create *Prx1-Pbx1-Gli3* mutant mice, floxed-*Pbx1-Gli3* mice were mated with *Prx1-Cre-Pbx1-Gli3* mutant mice. As a control, *Prx1-Cre*-negative embryos were used.

For genetic lineage analysis and FACS experiments, either *Col2A1-CreER*^{T2} or *Sox9-CreER*^{T2} mice were crossed with *Rosa26-tdTomato* reporter mice. Induction of Cre recombinase was performed at various pregnancy stages by administration of 0.03 mg/g tamoxifen/body weight in corn oil by oral gavage (stock concentration was 5 mg/ml).

Skeletal preparations

Cartilage and bone in whole mouse embryos were visualized, after skinning and disemboweling, by staining with Alcian Blue (Millipore Sigma, A5268) and Alizarin Red S (Millipore Sigma, A5533) and clarification of soft tissue with 3% potassium hydroxide and 100% glycerol (McLeod, 1980).

Paraffin sections

For preparation of paraffin sections, embryos were harvested at various ages, dissected and fixed in 4% paraformaldehyde (PFA)/PBS at 4°C overnight. After fixation, tissues were dehydrated in an ethanol series to 100% and embedded in paraffin. The embedded tissues were sectioned at a thickness of 7 µm using a microtome (LM2235, Leica) and mounted onto slides.

O.C.T-embedded sections

For preparation of O.C.T-embedded sections, embryos were harvested at various ages, dissected and fixed in 1% PFA/PBS at 4°C overnight. Fixed embryos were then dehydrated in 30% sucrose overnight at 4°C. Next, samples were dissected, soaked in O.C.T (Tissue-Tek) for 30-60 min and then frozen in O.C.T. Frozen samples were sectioned at a thickness of 10 µm using a cryostat (CM3050S, Leica) and mounted onto slides.

FISH

FISH on paraffin sections were performed using *Hoxd11* digoxigenin (DIG)-labeled RNA probe (Shwartz and Zelzer, 2014). Probe was detected using anti-DIG-POD (1:300, 11207733910, Roche), followed by Cy3-tyramide labeled fluorescent dyes, according to the instructions of the TSA Plus Fluorescent Systems Kit (PerkinElmer). Finally, slides were counter-stained using DAPI (1:1000, D9542, Millipore Sigma).

Development (2019) 146, dev167882. doi:10.1242/dev.167882

Immunofluorescence staining

For immunofluorescence staining for SOX9 and COL2A1, 7 µm-thick paraffin sections of embryo limbs were deparaffinized and rehydrated in water. Antigen was then retrieved in 10 mM citrate buffer (pH 6.0), boiled and cooked for 10 min in a microwave oven. In order to block non-specific binding of immunoglobulin, sections were incubated with 7% goat serum, 1% bovine serum albumin (BSA) dissolved in PBT (PBS+0.1% Tween 20) for 60 min at room temperature. Following blockage, sections were incubated overnight at 4°C with primary anti-SOX9 antibody (1:150, AB5535, Millipore Sigma). Then, sections were washed in PBT and incubated with Cy3-conjugated secondary fluorescent antibodies (1:100, 711-165-215, Jackson ImmunoResearch) for 60 min at room temperature. After staining for SOX9, slides were washed in PBT and fixed in 4% PFA at room temperature for 10 min. Then, slides were incubated with proteinase K (Millipore Sigma, P9290), washed and post-fixed again in 4% PFA. Next, sections were washed and incubated overnight at 4°C with primary anti-COL2A1 antibody (1:50, II-II6B3, the Developmental Studies Hybridoma Bank). The next day, sections were washed in PBT and incubated with Cy2-conjugated secondary fluorescent antibodies (1:100; 715-225-150, Jackson ImmunoResearch) for 60 min at room temperature. Slides were mounted with Immu-mount aqueous-based mounting medium (Thermo Fisher Scientific).

For immunofluorescence staining for SOX9 and *ScxGFP*, 10 µm-thick cryostat sections of embryo limbs endogenously labeled for *ScxGFP* were used. SOX9 immunofluorescence staining was performed as described above, but with omission of the antigen retrieval step, using primary SOX9 antibody and secondary Cy3-fluorescent antibodies.

For immunofluorescence staining for PBX1 and COL2A1, paraffin sections were used and antigen retrieval and blockage of non-specific binding were performed as described above. Endogenous peroxidase was quenched by incubation in 2% H_2O_2/PBS for 30 min at room temperature. Staining for PBX1 was performed using primary anti-PBX1 antibodies (1:400, C-4342, Cell Signaling Technology) followed by HRP-conjugated secondary antibodies (1:1000, 711-035-152, Jackson ImmunoResearch) and Cy3-tyramide labeled fluorescent dyes, according to the instructions of the TSA Plus Fluorescent Systems Kit (PerkinElmer). Subsequently, staining against COL2A1 was performed as described above.

For immunofluorescence staining for pSMAD1/5 and COL2A1, 7 µm-thick paraffin sections of embryo limbs were deparaffinized and rehydrated in water. For antigen retrieval, slides were incubated with proteinase K (Millipore Sigma, P9290) for 20 min at room temperature, washed and post-fixed again in 4% PFA. Endogenous peroxidase was quenched by incubation in 2% H_2O_2/PBS for 30 min at room temperature. Next, staining for pSMAD1/5 was performed using primary anti-pSMAD1/5/9 antibodies (1:200, CST-13820, Cell Signaling Technology) followed by biotin-conjugated secondary antibodies (1:100, 711-065-152, Jackson ImmunoResearch) and HRP-conjugated streptavidin (1:200, NEL750001EA, PerkinElmer). Finally, detection was performed using Cy3-tyramide labeled fluorescent dyes, according to the instructions of the TSA Plus Fluorescent Systems Kit (PerkinElmer). Subsequently, staining against COL2A1 was performed as described above.

BrdU staining and quantification

To examine cell proliferation, pregnant females were injected subcutaneously with 100 µg/g BrdU/body weight dissolved in PBS (stock concentration was 10 mg/ml) (B5002, Millipore Sigma). After 2 h of exposure, pregnant mice were scarified and the embryos were harvested, genotyped, fixated and embedded in paraffin. To detect BrdU-incorporated cells, immunostaining using primary anti-BrdU antibodies (1:200, MCA2060, Bio-Rad) and secondary Cy3-conjugated fluorescent antibodies (1:100; 712-165-153, Jackson ImmunoResearch) was performed on 7 µm-thick paraffin sections. Antigen retrieval using 10 mM citrate buffer (pH 6.0) and counterstaining for SOX9 were performed as described above. Quantification of BrdU-stained cells was performed using sections collected from three embryos from three different litters. From each embryo, at least two sections were used for statistical analysis ($n \geq 6$). In each section, the number of $Sox9^+$ and $Sox9^+$/$BrdU^+$ stained cells were counted within the area of the greater and deltoid tuberosities. The fraction of proliferative cells was calculated for each group and the difference between control and mutant embryos was tested using Student's *t*-test. Statistical significance was determined as $P \leq 0.05$.

TUNEL staining for detection of apoptosis

To examine cell death, we performed a TUNEL assay using ApopTag plus peroxidase *in situ* apoptosis kit (S7101, Millipore Sigma) according to the user guide supplied by the manufacturer, except for the use of DAB as the main peroxidase substrate. As a substitute, we used Cy3-tyramide labeled fluorescent dyes, according to the instructions of the TSA Plus Fluorescent Systems Kit (PerkinElmer). Finally, counterstaining was performed using DAPI (1:1000, D9542, Millipore Sigma).

Tissue clearing for light-sheet fluorescence microscopy

For whole-mount imaging, samples were first cleared and immunostained using the PACT-decal technique (Treweek et al., 2015; Yang et al., 2014). Briefly, either *Col2A1-CreER^{T2}*- or *Sox9-CreER^{T2}* mice were crossed with *Rosa26-tdTomato* reporter mice. Following tamoxifen administration at E11.5 (*Col2A1-CreER^{T2}*) or E10.5 (*Sox9-CreER^{T2}*), as described above, embryos were harvested at E15.5 or E14.5, respectively. Embryos were dissected and fixed in 1% PFA/PBS at 4°C overnight. Next, samples were washed in PBTx (PBS+0.1% Triton X-100+0.01% sodium azide) at room temperature, then embedded into a hydrogel of 4% (wt/vol) acrylamide in 1× PBS with 0.25% thermal initiator 2,2′-azobis[2-(2-imidazolin-2-yl)propane] dihydrochloride (VA-044, FUJIFILM-Wako). The hydrogel was allowed to polymerize at 37°C for 5 h. The samples were removed from the hydrogel, washed in PBTx, and moved to 10% sodium dodecyl sulfate (SDS) with 0.01% sodium azide, shaking at 37°C for 3 days, changing the SDS solution each day. Samples were washed four times with 1× PBTx at room temperature over the course of 24 h and fixed in 4% PFA at room temperature for 10 min. Then, samples were incubated with proteinase K (Millipore Sigma, P9290) for 30 min with shaking at 37°C, washed and post-fixed again in 4% PFA. To detect COL2A1, samples were first incubated with 5% goat serum dissolved in PBTx at 37°C overnight in order to block non-specific binding of immunoglobulin. Next, samples were incubated with primary COL2A1 antibodies (1:150, II-II6B3, the Developmental Studies Hybridoma Bank) in 2.5% goat serum/ PBTx shaking at 37°C for 3 days, changing the antibody solution each day. Samples were washed four times with 1× PBTx at room temperature over the course of 24 h. Next, samples were incubated with secondary Cy3 or Cy2 antibodies (1:150, 715-165-150 or 715-225-150, respectively, Jackson ImmunoResearch) in 2.5% goat serum/PBTx with shaking at 37°C overnight. Samples were washed again with four changes of 1× PBTx, and the refractive index (RI) of the sample was brought to 1.45 by submersion in a refractive index matching solution (RIMS) prepared by dissolving 35 g of Histodenz (Millipore Sigma, D2158) in 0.02 M phosphate buffer (74% wt/vol), and shaking gently at room temperature overnight. Finally, samples were embedded in 1% low gelling Agarose (Millipore Sigma, A9414) in PBS in a glass capillary, submerged in RIMS and stored in the dark at room temperature until imaging.

Light-sheet fluorescence microscopy

The cleared samples were imaged with a Zeiss Lightsheet Z.1 microscope. For each limb, a low-resolution image of the entire limb was taken with the 20× Clarity lens at a zoom of 0.36. Light-sheet fusion of images was done if necessary (Zen software, Zeiss). Tile stitching and 3D-image reconstruction was performed using Arivis Vision4D (Arivis) and Imaris (Bitplane) Software.

FACS

Flow cytometry analysis and sorting were performed on a BD FACS AriaIII instrument (BD Immunocytometry Systems) equipped with a 488, 407, 561 and 633 nm lasers, using a 70 µm nozzle, controlled by BD FACS Diva software v8.0.1 (BD Biosciences), at the Weizmann Institute of Science Flow Cytometry Core Facility. Further analysis was performed using FlowJo software v10.2 (Tree Star).

For collection of cells, *Sox9-CreER^{T2}-tdTomato;ScxGFP* mice were crossed with *Rosa26-tdTomato;ScxGFP* reporter mice. Embryos were harvested at E13.5 following tamoxifen administration at E12.0, as described above. Forelimbs were dissected and suspended in cold PBS using 15 ml tubes.

To extract cells from tissues, PBS was replaced with 1 ml pre-heated 0.05% trypsin (0.25% Trypsin EDTA solution A, Biological Industries) diluted in DMEM media (Thermo Fisher Scientific) and incubated for

Development (2019) 146, dev167882. doi:10.1242/dev.167882

15 min at 37°C, with gentle agitation every 5 min. Tissues were then dissociated by vigorous pipetting using 1 ml tips. Next, 4 ml of DMEM supplemented with 10% fetal bovine serum (FBS) and 1% penicillin-streptomycin solution (Biological Industries) was added and cell suspensions were filtered into a 15 ml tube using a syringe and a 40 µm filter net. Finally, tubes were centrifuged at 1000 rpm (90 ***g***) for 7 min, supernatant was removed and cells were resuspended in 1 ml of cold PBS and used immediately for FACS.

Single-stained GFP and tdTomato control cells were used for configuration and determining gate boundaries. Live cells were gated by size and granularity using FSC-A versus SSC-A and according to staining with propidium iodide (PI, 1 µg/ml) and DAPI (1 µg/ml). FSC-W versus FSC-A was used to further distinguish single cells. In addition, unstained, GFP-stained only and tdTomato-stained only cells were mixed in various combinations to verify that the analysis excluded false-positive doublets.

Bulk MARS-Seq

Purified RNA from FACS-isolated *Sox9*$^{+}$/*Scx*$^{+}$ cell samples was used for library preparation according to a standard MARS-Seq protocol (Jaitin et al., 2014). Library quality was analyzed by a 2200 TapeStation instrument (Agilent Technologies, data not shown). The experiment produced libraries of high quality and sufficient quantity. Libraries were subsequently sequenced by Illumina NextSeq 500.

Bioinformatic analysis

The analysis was performed as described by Köster and Rahmann (2012). Briefly, a unique molecular identifier (UMI) sequence present in the R2 read was inserted in the read name of R1 sequence file using a python script. Cutadapt (Martin, 2011) was used to trim low quality and poly A/T and adapter sequences (-a AGATCGGAAGAGCACACGTCTGAACTCCAG-TCAC -a "A{100}" -a "T{100}" –times 2 -q 20 -m 30). Sequences were mapped using TopHat2 to mouse genome build mm10 (Kim et al., 2013). UMI information was integrated into the BAM files as tags, using a python script. The BAM file was converted to SAM format using Samtools (Li et al., 2009). Duplicate reads were marked and filtered based on having the same UMI and mapping to the same gene, using a python script. UMI counts per gene were calculated using modified HTSeq-count script (Anders et al., 2014) and a RefSeq gtf file (downloaded from igenomes UCSC), which was modified to contain a window surrounding the 3′ UTR.

DESeq2 (Love et al., 2014) was used for normalization and to detect differentially expressed genes based on negative binomial distribution and a generalized linear regression model. The model used contained two factors: olecranon or deltoid tuberosity *Sox9*$^{+}$/*Scx*$^{+}$ precursors and a batch factor. Genes were considered differentially expressed if the difference in expression between at least two sample types was statistically significant after adjustment with the fdrtool package (adjusted P-value≤0.05) (Strimmer, 2008). After filtering based on expression levels (sum normalized count in all samples greater than 10 and maximum expression level higher than 5), clustering of the standardized normalized counts was carried out using click algorithm (Expander package, Ulitsky et al., 2010). Further analysis was performed using GSEA (Broad institute) and Ingenuity (IPA).

Acknowledgements

We thank N. Konstantin for expert editorial assistance, and members of the Zelzer laboratory for their advice and suggestions; R. Schweitzer for providing the *ScxGFP*, *Scx-Cre* and *Sox9-Cre* mice, L. Selleri for providing the *Pbx1*^{null} and *Pbx2*^{null} mice, and H. Akiyama for providing the *Sox9-CreER*^{T2} mice; and O. Golani from the Weizmann Institute Department of Life Sciences Core Facilities for her guidance and assistance in analyzing and designing the experiments. Light sheet imaging was made possible thanks to the De Picciotto-Lesser Cell Observatory in memory of Wolf and Ruth Lesser of the MICC. We thank C. Vega from the Weizmann Institute Department of Design, Photography and Printing for designing the graphic model.

Competing interests

The authors declare no competing or financial interests.

Author contributions

Conceptualization: S.E., E.Z.; Methodology: S.E., S. Kult, S.R., S. Krief, N.F., K.M.P., D.L., T.-M.S., Y.A., E.Z.; Software: D.L.; Validation: S.E., S. Kult, S.R., S. Krief, N.F., D.L., T.-M.S., Y.A., D.M.W.; Formal analysis: D.L., T.-M.S.; Investigation: S.E., S. Kult, S.R., S. Krief, N.F., K.M.P.; Resources: N.F., K.M.P., D.M.W.; Data curation: D.L., T.-M.S.; Writing - original draft: S.E., E.Z.; Writing - review & editing: D.L., T.-M.S., D.M.W.; Visualization: S.E., Y.A.; Supervision: E.Z.; Project administration: E.Z.; Funding acquisition: E.Z.

Funding

This study was supported by grants from the National Institutes of Health (R01 AR055580), the European Research Council (310098), the Jeanne and Joseph Nissim Foundation for Life Sciences Research, the Y. Leon Benoziyo Institute for Molecular Medicine, Beth Rom-Rymer, the Estate of David Levinson, the Jaffe Bernard and Audrey Foundation, the Georges Lustgarten Cancer Research Fund, the David and Fela Shapell Family Center for Genetic Disorders, the David and Fela Shapell Family Foundation INCPM Fund for Preclinical Studies, and the Estate of Bernard Bishin for the WIS-Clalit Program. Deposited in PMC for release after 12 months.

Data availability

The data discussed in this publication have been deposited in NCBI's Gene Expression Omnibus under accession number GSE129820.

Supplementary information

Supplementary information available online at
http://dev.biologists.org/lookup/doi/10.1242/dev.167882.supplemental

References

Anders, S., Pyl, P. T. and Huber, W. (2014). HTSeq – a Python framework to work with high-throughput sequencing data. *Bioinformatics* **31**, 166-169. doi:10.1093/bioinformatics/btu638

Archer, M., Beck, R., Gott, M., Hand, S., Godthelp, H. and Black, K. (2011). Australia's first fossil marsupial mole (Notoryctemorphia) resolves controversies about their evolution and palaeoenvironmental origins. *Proc. R. Soc. B* **278**, 1498-1506. doi:10.1098/rspb.2010.1943

Berendsen, A. D. and Olsen, B. R. (2015). Bone development. *Bone* **80**, 14-18. doi:10.1016/j.bone.2015.04.035

Blaess, S., Stephen, D. and Joyner, A. L. (2008). Gli3 coordinates three-dimensional patterning and growth of the tectum and cerebellum by integrating Shh and Fgf8 signaling. *Development* **135**, 2093-2103. doi:10.1242/dev.015990

Blitz, E., Viukov, S., Sharir, A., Shwartz, Y., Galloway, J. L., Pryce, B. A., Johnson, R. L., Tabin, C. J., Schweitzer, R. and Zelzer, E. (2009). Bone ridge patterning during musculoskeletal assembly is mediated through SCX regulation of Bmp4 at the tendon-skeleton junction. *Dev. Cell* **17**, 861-873. doi:10.1016/j.devcel.2009.10.010

Blitz, E., Sharir, A., Akiyama, H. and Zelzer, E. (2013). Tendon-bone attachment unit is formed modularly by a distinct pool of Scx- and Sox9-positive progenitors. *Development* **140**, 2680-2690. doi:10.1242/dev.093906

Boulet, A. M. and Capecchi, M. R. (2004). Multiple roles of Hoxa11 and Hoxd11 in the formation of the mammalian forelimb zeugopod. *Development* **131**, 299-309. doi:10.1242/dev.00936

Cain, C. J., Gaborit, N., Lwin, W., Barruet, E., Ho, S., Bonnard, C., Hamamy, H., Shboul, M., Reversade, B., Kayserili, H., et al. (2016). Loss of Iroquois homeobox transcription factors 3 and 5 in osteoblasts disrupts cranial mineralization. *Bone Rep.* **5**, 86-95. doi:10.1016/j.bonr.2016.02.005

Capellini, T. D. (2006). Pbx1/Pbx2 requirement for distal limb patterning is mediated by the hierarchical control of Hox gene spatial distribution and Shh expression. *Development* **133**, 2263-2273. doi:10.1242/dev.02395

Cervantes-Diaz, F., Contreras, P. and Marcellini, S. (2017). Evolutionary origin of endochondral ossification: the transdifferentiation hypothesis. *Dev. Genes Evol.* **227**, 121-127. doi:10.1007/s00427-016-0567-y

Colasanto, M. P., Eyal, S., Mohassel, P., Bamshad, M., Bonnemann, C. G., Zelzer, E., Moon, A. M. and Kardon, G. (2016). Development of a subset of forelimb muscles and their attachment sites requires the ulnar-mammary syndrome gene *Tbx3*. *Dis. Model. Mech.* **9**, 1257-1269. doi:10.1242/dmm.025874

Davis, A. P. and Capecchi, M. R. (1994). Axial homeosis and appendicular skeleton defects in mice with a targeted disruption of hoxd-11. *Development* **120**, 2187-2198.

Eyal, S., Blitz, E., Shwartz, Y., Akiyama, H., Schweitzer, R. and Zelzer, E. (2015). On the development of the patella. *Development* **142**, 1831-1839. doi:10.1242/dev.121970

Eyal, S., Rubin, S., Krief, S., Levin, L. and Zelzer, E. (2019). Common cellular origin and diverging developmental programs for different sesamoid bones. *Development* **146**, dev167452. doi:10.1242/dev.167452

Ficara, F., Murphy, M. J., Lin, M. and Cleary, M. L. (2008). Pbx1 regulates self-renewal of long-term hematopoietic stem cells by maintaining their quiescence. *Cell Stem Cell* **2**, 484-496. doi:10.1016/j.stem.2008.03.004

Galli, A., Robay, D., Osterwalder, M., Bao, X., Bénazet, J.-D., Tariq, M., Paro, R., Mackem, S. and Zeller, R. (2010). Distinct roles of Hand2 in initiating polarity and

posterior Shh expression during the onset of mouse limb bud development. *PLoS Genet.* **6**, e1000901. doi:10.1371/journal.pgen.1000901

Gross, S., Krause, Y., Wuelling, M. and Vortkamp, A. (2012). Hoxa11 and Hoxd11 regulate chondrocyte differentiation upstream of Runx2 and Shox2 in mice. *PLoS ONE* **7**, e43553. doi:10.1371/journal.pone.0043553

Hasson, P., Del Buono, J. and Logan, M. P. (2007). Tbx5 is dispensable for forelimb outgrowth. *Development* **134**, 85-92. doi:10.1242/dev.02622

Holmberg, J., Ingner, G., Johansson, C., Leander, P. and Hjalt, T. A. (2008). PITX2 gain-of-function induced defects in mouse forelimb development. *BMC Dev. Biol.* **8**, 25. doi:10.1186/1471-213X-8-25

Hsieh-Li, H. M., Witte, D. P., Weinstein, M., Branford, W., Li, H., Small, K. and Potter, S. S. (1995). Hoxa11 structure, extensive antisense transcription, and function in male and female fertility. *Development* **121**, 1373-1385.

Jaitin, D. A., Kenigsberg, E., Keren-Shaul, H., Elefant, N., Paul, F., Zaretsky, I., Mildner, A., Cohen, N., Jung, S. and Tanay, A. (2014). Massively parallel single-cell RNA-seq for marker-free decomposition of tissues into cell types. *Science* **343**, 776-779. doi:10.1126/science.1247651

Johnson, D. R. (1967). Extra-toes: a new mutant gene causing multiple abnormalities in the mouse. *Development* **17**, 543-581.

Kawakami, Y., Rodriguez-León, J. and Belmonte, J. C. I. (2006). The role of TGFβs and Sox9 during limb chondrogenesis. *Curr. Opin. Cell Biol.* **18**, 723-729. doi:10.1016/j.ceb.2006.10.007

Kim, D., Pertea, G., Trapnell, C., Pimentel, H., Kelley, R. and Salzberg, S. L. (2013). TopHat2: accurate alignment of transcriptomes in the presence of insertions, deletions and gene fusions. *Genome Biol.* **14**, R36. doi:10.1186/gb-2013-14-4-r36

Köster, J. and Rahmann, S. (2012). Snakemake – a scalable bioinformatics workflow engine. *Bioinformatics* **28**, 2520-2522. doi:10.1093/bioinformatics/bts480

Koyama, E., Yasuda, T., Minugh-Purvis, N., Kinumatsu, T., Yallowitz, A. R., Wellik, D. M. and Pacifici, M. (2010). Hox11 genes establish synovial joint organization and phylogenetic characteristics in developing mouse zeugopod skeletal elements. *Development* **137**, 3795-3800. doi:10.1242/dev.053447

Kronenberg, H. M. (2003). Developmental regulation of the growth plate. *Nature* **423**, 332-336. doi:10.1038/nature01657

Lessa, E. P., Vassallo, A. I., Verzi, D. H. and Mora, M. S. (2008). Evolution of morphological adaptations for digging in living and extinct ctenomyid and octodontid rodents. *Biol. J. Linn. Soc.* **95**, 267-283. doi:10.1111/j.1095-8312.2008.01057.x

Li, H., Handsaker, B., Wysoker, A., Fennell, T., Ruan, J., Homer, N., Marth, G., Abecasis, G., Durbin, R. and **1000 Genome Project Data Processing Subgroup**. (2009). The sequence alignment/Map format and SAMtools. *Bioinformatics* **25**, 2078-2079. doi:10.1093/bioinformatics/btp352

Li, D., Sakuma, R., Vakili, N. A., Mo, R., Puviindran, V., Deimling, S., Zhang, X., Hopyan, S. and Hui, C.-C. (2014). Formation of proximal and anterior limb skeleton requires early function of Irx3 and Irx5 and is negatively regulated by Shh signaling. *Dev. Cell* **29**, 233-240. doi:10.1016/j.devcel.2014.03.001

Litingtung, Y., Dahn, R. D., Li, Y., Fallon, J. F. and Chiang, C. (2002). Shh and Gli3 are dispensable for limb skeleton formation but regulate digit number and identity. *Nature* **418**, 979. doi:10.1038/nature01033

Logan, M., Martin, J. F., Nagy, A., Lobe, C., Olson, E. N. and Tabin, C. J. (2002). Expression of Cre recombinase in the developing mouse limb bud driven by a Prxl enhancer. *Genesis* **33**, 77-80. doi:10.1002/gene.10092

Long, F. and Ornitz, D. M. (2013). Development of the Endochondral Skeleton. *Cold Spring Harbor Perspect. Biol.* **5**, a008334. doi:10.1101/cshperspect.a008334

Love, M. I., Huber, W. and Anders, S. (2014). Moderated estimation of fold change and dispersion for RNA-seq data with DESeq2. *Genome Biol.* **15**, 550. doi:10.1186/s13059-014-0550-8

Madisen, L., Zwingman, T. A., Sunkin, S. M., Oh, S. W., Zariwala, H. A., Gu, H., Ng, L. L., Palmiter, R. D., Hawrylycz, M. J., Jones, A. R. et al. (2010). A robust and high-throughput Cre reporting and characterization system for the whole mouse brain. *Nat. Neurosci.* **13**, 133-140. doi:10.1038/nn.2467

Martin, M. (2011). Cutadapt removes adapter sequences from high-throughput sequencing reads. *EMBnet. J.* **17**. doi:10.14806/ej.17.1.200

McHenry, H. M. and Corruccini, R. S. (1975). Distal humerus in hominoid evolution. *Folia Primatol.* **23**, 227-244. doi:10.1159/000155673

McLeod, M. J. (1980). Differential staining of cartilage and bone in whole mouse fetuses by Alcian Blue and Alizarin Red S. *Teratology* **22**, 299-301. doi:10.1002/tera.1420220306

Mercader, N., Selleri, L., Criado, L. M., Pallares, P., Parras, C., Cleary, M. L. and Torres, M. (2009). Ectopic Meis1 expression in the mouse limb bud alters PD patterning in a Pbx1-independent manner. *Int. J. Dev. Biol.* **53**, 1483-1494. doi:10.1387/ijdb.072430nm

Milne, N. and O'Higgins, P. (2012). Scaling of form and function in the xenarthran femur: a 100-fold increase in body mass is mitigated by repositioning of the third trochanter. *Proc. R. Soc. B* **279**, 3449-3456. doi:10.1098/rspb.2012.0593

Nakamura, E., Nguyen, M.-T. and Mackem, S. (2006). Kinetics of tamoxifen-regulated Cre activity in mice using a cartilage-specific CreERT to assay temporal activity windows along the proximodistal limb skeleton. *Dev. Dyn.* **235**, 2603-2612. doi:10.1002/dvdy.20892

Neufeld, S. J., Wang, F. and Cobb, J. (2014). Genetic interactions between Shox2 and Hox genes during the regional growth and development of the mouse limb. *Genetics* **198**, 1117-1126. doi:10.1534/genetics.114.167460

Olsen, B. R., Reginato, A. M. and Wang, W. (2000). Bone development. *Annu. Rev. Cell Dev. Biol.* **16**, 191-220. doi:10.1146/annurev.cellbio.16.1.191

Polly, P. D. (2007). Limbs in mammalian evolution. In *Fins into Limbs: Evolution, Development and Transformation* (ed. B. K. Hall), pp. 245-268. University of Chicago Press.

Pryce, B. A., Brent, A. E., Murchison, N. D., Tabin, C. J. and Schweitzer, R. (2007). Generation of transgenic tendon reporters, ScxGFP and ScxAP, using regulatory elements of the scleraxis gene. *Dev. Dyn.* **236**, 1677-1682. doi:10.1002/dvdy.21179

Retting, K. N., Song, B., Yoon, B. S. and Lyons, K. M. (2009). BMP canonical Smad signaling through Smad1 and Smad5 is required for endochondral bone formation. *Development* **136**, 1093-1104. doi:10.1242/dev.029926

Salton, J. A. and Sargis, E. J. (2008). Evolutionary morphology of the Tenrecoidea (Mammalia) forelimb skeleton. In *Mammalian Evolutionary Morphology* (ed. E. J. Sargis and M. Dagosto), pp. 51-71. Dordrecht: Springer Netherlands.

Salton, J. A. and Sargis, E. J. (2009). Evolutionary morphology of the Tenrecoidea (Mammalia) hindlimb skeleton. *J. Morphol.* **270**, 367-387. doi:10.1002/jmor.10697

Selleri, L., Depew, M. J., Jacobs, Y., Chanda, S. K., Tsang, K. Y., Cheah, K. S., Rubenstein, J. L., O'Gorman, S. and Cleary, M. L. (2001). Requirement for Pbx1 in skeletal patterning and programming chondrocyte proliferation and differentiation. *Development* **128**, 3543-3557.

Selleri, L., DiMartino, J., van Deursen, J., Brendolan, A., Sanyal, M., Boon, E., Capellini, T., Smith, K. S., Rhee, J., Popperl, H. et al. (2004). The TALE Homeodomain protein Pbx2 is not essential for development and long-term survival. *Mol. Cell. Biol.* **24**, 5324-5331. doi:10.1128/MCB.24.12.5324-5331.2004

Shwartz, Y. and Zelzer, E. (2014). Nonradioactive in situ hybridization on skeletal tissue sections. *Skelet. Dev. Repair* **1130**, 203-215. doi:10.1007/978-1-62703-989-5_15

Soeda, T., Deng, J. M., de Crombrugghe, B., Behringer, R. R., Nakamura, T. and Akiyama, H. (2010). Sox9-expressing precursors are the cellular origin of the cruciate ligament of the knee joint and the limb tendons. *Genesis* **48**, 635-644. doi:10.1002/dvg.20667

Strimmer, K. (2008). fdrtool: a versatile R package for estimating local and tail area-based false discovery rates. *Bioinformatics* **24**, 1461-1462. doi:10.1093/bioinformatics/btn209

Sugimoto, Y., Takimoto, A., Akiyama, H., Kist, R., Scherer, G., Nakamura, T., Hiraki, Y. and Shukunami, C. (2013). Scx+/Sox9+ progenitors contribute to the establishment of the junction between cartilage and tendon/ligament. *Development* **140**, 2280-2288. doi:10.1242/dev.096354

Swinehart, I. T., Schlientz, A. J., Quintanilla, C. A., Mortlock, D. P. and Wellik, D. M. (2013). Hox11 genes are required for regional patterning and integration of muscle, tendon and bone. *Development* **140**, 4574-4582. doi:10.1242/dev.096693

Treweek, J. B., Chan, K. Y., Flytzanis, N. C., Yang, B., Deverman, B. E., Greenbaum, A., Lignell, A., Xiao, C., Cai, L., Ladinsky, M. S. et al. (2015). Whole-body tissue stabilization and selective extractions via tissue-hydrogel hybrids for high-resolution intact circuit mapping and phenotyping. *Nat. Protoc.* **10**, 1860-1896. doi:10.1038/nprot.2015.122

Ulitsky, I., Maron-Katz, A., Shavit, S., Sagir, D., Linhart, C., Elkon, R., Tanay, A., Sharan, R., Shiloh, Y. and Shamir, R. (2010). Expander: from expression microarrays to networks and functions. *Nat. Protoc.* **5**, 303. doi:10.1038/nprot.2009.230

Wellik, D. M. and Capecchi, M. R. (2003). Hox10 and Hox11 genes are required to globally pattern the mammalian skeleton. *Science* **301**, 363-367. doi:10.1126/science.1085672

Xu, B. and Wellik, D. M. (2011). Axial Hox9 activity establishes the posterior field in the developing forelimb. *Proc. Natl Acad. Sci. USA* **108**, 4888-4891. doi:10.1073/pnas.1018161108

Yang, B., Treweek, J. B., Kulkarni, R. P., Deverman, B. E., Chen, C.-K., Lubeck, E., Shah, S., Cai, L. and Gradinaru, V. (2014). Single-cell phenotyping within transparent intact tissue through whole-body clearing. *Cell* **158**, 945-958. doi:10.1016/j.cell.2014.07.017

Yang, Y., Topol, L., Lee, H. and Wu, J. (2003). Wnt5a and Wnt5b exhibit distinct activities in coordinating chondrocyte proliferation and differentiation. *Development* **130**, 1003-1015. doi:10.1242/dev.00324

Yashiro, K., Zhao, X., Uehara, M., Yamashita, K., Nishijima, M., Nishino, J., Saijoh, Y., Sakai, Y. and Hamada, H. (2004). Regulation of retinoic acid distribution is required for proximodistal patterning and outgrowth of the developing mouse limb. *Dev. Cell* **6**, 411-422. doi:10.1016/S1534-5807(04)00062-0

Zhao, Q., Eberspaecher, H., Lefebvre, V. and de Crombrugghe, B. (1997). Parallel expression ofSox9 andCol2a1 in cells undergoing chondrogenesis. *Dev. Dyn.* **209**, 377-386. doi:10.1002/(SICI)1097-0177(199708)209:4<377::AID-AJA5>3.0.CO;2-F